




Article

Response Modification Factors for Multi-Span Reinforced Concrete Bridges in Pakistan

Muhammad Jamal Butt ¹, Muhammad Waseem ², Muhammad Ali Sikandar ^{3,*} , Bakht Zamin ³, Mahmood Ahmad ^{4,*}  and Mohanad Muayad Sabri Sabri ⁵ 

- ¹ Department of Civil Engineering & Technology, Qurtuba University of Science & IT, Dera Ismail Khan 29050, Pakistan; emjb@qurtuba.edu.pk
- ² Department of Civil Engineering, University of Engineering & Technology, Peshawar 25120, Pakistan; m.waseem@uetpeshawar.edu.pk
- ³ Department of Civil Engineering, CECOS University of Technology and Emerging Sciences, Peshawar 25120, Pakistan; bakht@cecos.edu.pk
- ⁴ Department of Civil Engineering, University of Engineering and Technology Peshawar (Bannu Campus), Bannu 28100, Pakistan
- ⁵ Peter the Great St. Petersburg Polytechnic University, 195251 St. Petersburg, Russia; mohanad.m.sabri@gmail.com
- * Correspondence: msikandar@cecos.edu.pk (M.A.S.); ahmadm@uetpeshawar.edu.pk (M.A.)

Abstract: In Pakistan, updated codes covering seismic provisions for reinforced concrete bridges do not exist. The majority of the bridge design uses different versions of AASTHO-LRFD provisions. Response modification factors recommended for usage in these codes are primarily for bridges derived from conditions and bridges in the United States of America. This research focuses on the seismic assessment of three real multi-spans simply supported reinforced concrete bridges in Pakistan having multiple bents. This typology of bridges is very common in Pakistan. Non-linear static pushover analysis is performed to derive seismic capacity curves for these bridges, which were used to compute response modification factors. The study results show that response modification factors vary between 4.50 and 5.0 for the bridges in the longitudinal and transverse directions. The results of this work may serve as input in developing the seismic design code of bridges in Pakistan.

Keywords: reinforced concrete bridge; response modification factor; multi-spans; multiple bents; seismic design



Citation: Butt, M.J.; Waseem, M.; Sikandar, M.A.; Zamin, B.; Ahmad, M.; Muayad Sabri Sabri, M. Response Modification Factors for Multi-Span Reinforced Concrete Bridges in Pakistan. *Buildings* **2022**, *12*, 921. <https://doi.org/10.3390/buildings12070921>

Academic Editors: Weiping Wen and Duofa Ji

Received: 26 May 2022

Accepted: 24 June 2022

Published: 29 June 2022

Publisher's Note: MDPI stays neutral with regard to jurisdictional claims in published maps and institutional affiliations.



Copyright: © 2022 by the authors. Licensee MDPI, Basel, Switzerland. This article is an open access article distributed under the terms and conditions of the Creative Commons Attribution (CC BY) license (<https://creativecommons.org/licenses/by/4.0/>).

1. Introduction

There are approximately 6000 bridges on the national highways of Pakistan, and 67% of these were built before 1980. The seismic provisions followed for designing bridges in Pakistan are known as the West Pakistan Highway Code (WPHC) [1]. The WPHC was adopted from AASTHO (1961). However, since then, the WPHC was never updated. Instead, different versions of AASTHO-LRFD codes were consulted to design bridges. In the WPHC, the design base lateral force equals 2% to 6% of the seismic weight (i.e., 0.02 to 0.06 W). However, it lacks a reliable link between the site seismic hazard and design base lateral force. Kawashima [2] proposed seismic isolation technology for highway bridges. After the Kobe 1995 earthquake event in Japan, the author proposed guidelines and specifications for this technique. Sakellariadis et al. [3] revisited the collapse of the 18-span bridge during the tragic seismic event of Kobe in Japan in 1995. Putra et al. [4] conducted a case study of risk analysis of seismic bridge damage after the Lombok and Palu earthquakes in Indonesia. The authors performed an on-site visual inspection of 38 bridges and reported several damages to the bridges. Memari et al. [5] evaluated the seismic response of five existing bridge piers in the eastern region of the US seismic zone. The AASTHO-LRFD suggests seismic hazard having a return period of 1000 years for calculating

seismic actions for bridges. However, such seismic hazard maps are not available to date, which will lead to great destruction because significant energy is released during seismic events [6]. In a case study of the Tawarayama Bridge under the 2016 Kumamoto earthquake, Aye et al. [7] reported damage mechanisms based on seismic response analysis induced by an earthquake in a plate girder bridge. The Halabjah earthquake, which struck Iraq in November 2017 and damaged numerous bridge piers and commercial buildings, prompted Al-taie et al. [8] to conduct a case study about the seismic risks associated with Iraqi soil. The seismic hazard map of Pakistan was updated with the advent of the Building Code of Pakistan (BCP-SP-, 2007) [9]. However, this suggests values for peak ground acceleration (PGA) having a 10% probability of exceedance in 50 years within 475 years of the return period. Recently, S. Khan and Waseem [10] developed relevant latest probabilistic seismic hazard analysis (PSHA) maps for various return periods to evaluate Pakistan seismic zones. R. Khan et al. [11] conducted a study of the existing nine precast bridges to assess the vulnerability of bridges in Karachi to seismic ground motion.

Many improvements were made at the time by scientists and researchers to deal with seismic hazards, along with seismic site behavior. Numerous studies were conducted to depict structural behavior to dissipate seismic energy by causing adequate ductility to structures, such as in 1998 when AASHTO presented a report titled “Guide Specification for Seismic Isolation Design” [12]. Research results led to the establishment of an appropriate response modification factor for a substructure for seismic activity. The response modification factor given in the US codes FEMA1997, and UBC 1997 [13,14] are intended to account for both overstrength and ductility factors (ATC-1978) [15] available in the structural system to respond to design base earthquakes, which can be traced back to the empirical horizontal force factors adopted in the 1959 SEAOC Blue Book [16,17]. Inappropriate selection of R-factor may lead to underestimation or overestimation of design forces in the structure. For demonstration, the hazard maps developed by S. Khan and Waseem [10] suggested a maximum PGA of 0.51 g near the city of Quetta for a 975 year return period, rendering an elastic base shear demand of 0.51 W for a bridge having a fundamental time period of 1.0 s. Considering the maximum design base shear of 0.06 W for the same bridge, as per the suggestion of WPHC, this requires response modification factor R (demand) = $0.51/0.06 = 8.50$. Such a high value of a response modification factor (demand) may exceed the available response modification factor (capacity) of existing bridges. Nearly two decades ago, in the devastating earthquake that happened in Pakistan (the 8 October 2005 Kashmir earthquake), several bridges were either completely/partially collapsed or experienced extensive damage [1]. Many researchers have quantified this factor for appropriate seismic analysis and design.

In addition, many researchers have developed mechanical devices, isolators, and special ductile connections at beam columns or in bridge piers to dissipate seismic energy (R-factor) within the structure, such as in the USA, where many bridges reach their intended life rather than being replaced with new construction [18]. The authors proposed an apparatus, “Response Modification Apparatus”, which mechanically exhibits and amplifies adequate stiffness and damping of bridges. Gastineau et al. [19] likely further improved the Response Modification (RM) Apparatus for flexibility in member and in overall performance during vibrational effects. Routledge et al. [20] reported the case study of the Wigram-Magdala Bridge in New Zealand, which was difficult to retrofit due to the Christchurch earthquake. They concluded the performance of plastic hinge regions in typical reinforced concrete structures before developing low-damage ductile jointed systems to control damage in plastic hinge regions. Warn et al. [21] analyzed the twenty bilinear bridge isolator responses of various bridges to design a new seismic isolator for the seismic resilience of US bridges. Chavdar et al. [22] reported the response modification of the bridge, which is isolated by a lead rubber bearing pad (LRBs) due to change in low ambient temperature from 20 °C to −30°. Zhang et al. [23] followed up the seismic response of fault crossing simply supported precast bridge by fault rupture. The amplitude of numerical models were evaluated for permanent ground displacement. Correspondingly,

Bergami et al. [24] probed the near-fault event for the bridge and evaluated its response by ‘Incremental Modal Pushover Analysis’ (IMPA). China has rapidly progressed its high-speed railway (HSR) and lies in an earthquake-prone region. The HSR has faced seismic events ever since Guo et al. [25] proposed isolation bearing rather than common bearing to perform better in intense seismic events and working on the principle of “Equivalent energy-based design procedure (EEDP)”.

Seismic codes worldwide suggest a different value for ductility factor, e.g., a ductility factor value from 3 to 4 is given in the US seismic codes, a value of 3.0 is given in the seismic code of Japan, a value of 6.0 is given in the seismic code of New Zealand, and a value of 3.50 is given in the seismic code for Europe. The AASHTO recommends a response modification factor of 3.0 and 5.0 for longitudinal and transverse directions, respectively. Kappos et al. [26] analyzed existing reinforced concrete bridges with yielding piers and others having elastomeric bearing pads placed between piers and superstructures. For the first class of bridges, the response modification factor was quantified as the product of ductility and overstrength factors. This factor varied from 4.2 to 10.1 and 3.7 to 11.6 in longitudinal and transverse directions. For bridges with elastomeric bearing pads, the response modification factor was defined as the ratio of spectral acceleration (corresponding to the pertinent predominant period of the bridge) that causes failure to design spectral acceleration. This factor varied from 4.0 to 6.6 and 4.3 to 9.3 in the longitudinal and transverse directions, respectively. They expressed that this factor given in seismic code is possible but, in numerous cases, underestimates the realistic deformability and energy dissipation capacity of the bridges. Zahrai et al. [27] investigated five existing reinforced concrete bridges in Iran with elastomeric and lead rubber bearings and proposed that the average response modification factor for bridges with elastomeric bearing pad isolators is 3.89 and 4.91 in the longitudinal and transverse directions, respectively. For bridges with monolithic deck-column construction, response modification factors of 2.92 and 2.41 were obtained for longitudinal and transverse directions.

In the context of Pakistan, Waseem and Spacone [28] carried out the vulnerability of three RCC bridges in northern Pakistan. They derived the fragility functions of bridge components. However, R-factors were not evaluated for the bridges. S. Ali [29] evaluated the R-factor for the low-cost single pier of the bridges. This study is limited to the pier’s response only. Therefore, an attempt is made in this work to study the R-factor numerically for three bridges. This paper attempts to evaluate the R-factor values of bridges with ERB isolators to compare the results with those prescribed by the bridge design codes. According to AASHTO for seismic isolation design, the R-factor for all substructure elements of isolated bridges should be expressed in the AASHTO standard provisions for highway bridges. To investigate the R-factor for the most commonly found bridges in Pakistan, three simply supported spans in real RC bridges equipped with elastomeric bearing pads are analyzed using the static non-linear pushover analysis based on the Uang [30] approach.

2. Description of Reinforced Concrete Bridges

In Pakistan, the most common type of bridges constructed are simply supported superstructure multi-span RC bridges. In these bridges, the superstructure consists of an RC slab and prestressed girders. The substructure consists of circular single or multiple piers’ bent. The superstructure and superstructure are separated by elastomeric bearing pads. Expansion joints are provided with every span and at abutments. Three real bridges are considered in this work as candidates and representatives of the bridges from Pakistan.

2.1. Mingora Bridge

Mingora Bridge is located in the Khyber Pakhtunkhwa province in the north of Pakistan. It is a three-span RC bridge, and the two bents consist of three pier shafts and a rectangular cap beam described in Figure 1. (layout plans were provided by “AA Associates” consultant firm). The abutments of the bridge consist of RC walls with a pile cap foundation. The abutment of the bridge has a seating arrangement for the bearing

pad. Girder is pre-stressed, I-shaped, and placed over the bearing pads. Expansion joints of 25 mm are provided at every bent and abutment. Shear keys are provided between girders at the top of the cap beam to prevent lateral movement. A gap of 10 mm is provided between the girders and shear key, filled with polystyrene. Girders are connected with a diaphragm, and three diaphragms are provided in each span. The concrete compressive strength of girders is 34.47 MPa (5000 psi), while for all other members are 27.58 MPa (4000 psi). The bearing pads used in this bridge are rectangular with a laminated layer of steel. Its dimension is $400 \times 500 \times 46$ mm. The details of the Mingora Bridge are shown in Figure 1.

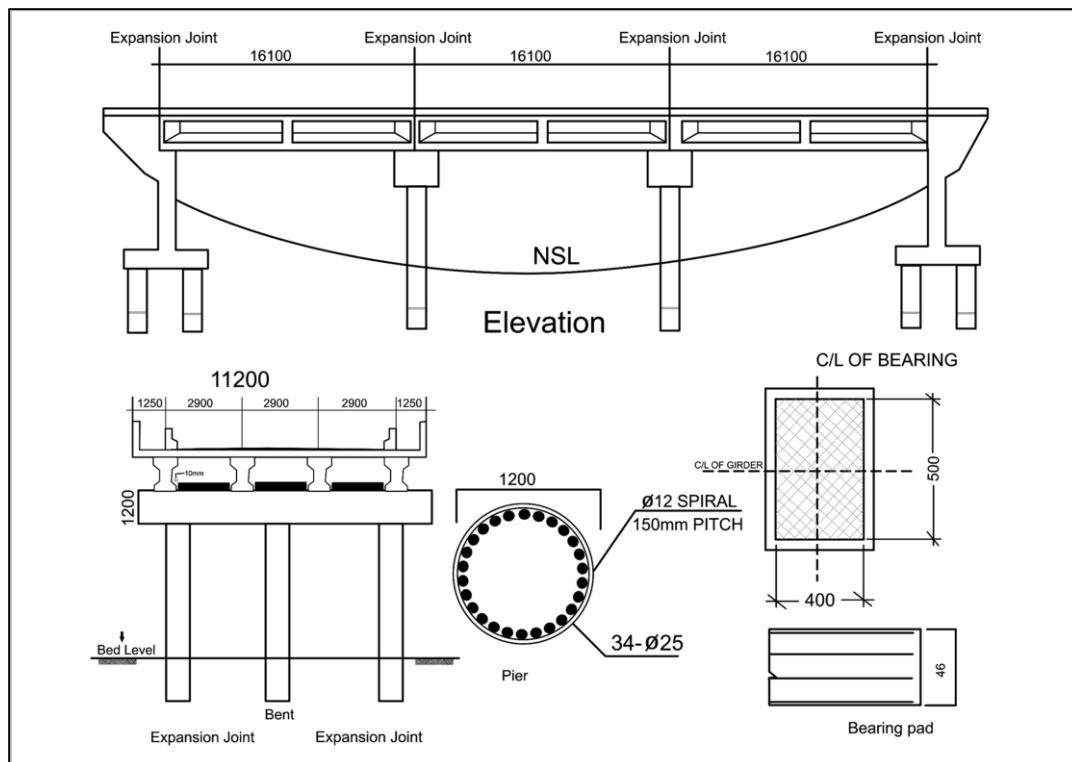


Figure 1. Mingora Bridge, Swat.

2.2. Shabqadar Bridge Charsadda

Shabqadar Bridge, located in the Charsadda district in the province of Khyber Pakhtunkhwa, is a ten-span, simply supported bridge with four multiple pier shaft bents described in the drawing (provided by “ABM Engineers” consultant firm). The bent possesses a solid circular column and a rectangular transom (cap beam). The abutment consists of an RCC wall supported on a foundation of pile cap and side wing walls. The abutment wall has seating arrangements for the bearing pad. The post-tensioned, I-shaped girders are supported at each end on the rectangular elastomeric bearing pad at a constant distance of 2600 mm. Five rectangular diaphragm beams are connected to hold four girders at each span, having a girder depth of 1800 mm. The symmetry of the members are the same throughout the bridge; each pier shaft is 1200 mm in diameter. The cap beam has a dimension of 1800 mm \times 1200 mm. Deck slab, girders at bent, and girders and abutment walls are separated by an expansion joint of 25 mm. The bearing pad is placed on a concrete pad, and a special epoxy grout helps to cement the pad. A shear block on the top of each column bent and the abutment is also built to prevent the lateral load and gap of 10 mm between the girder and shear block filled by polystyrene. The prestressed girder concrete cylinder compressive strength is 34.47 MPa (5000 psi), and the compressive strength of concrete in other members (deck slab, diaphragm, and pile) is 27.58 Mpa (4000 psi). Moreover, the compressive strength of the railing post, kerb, plank, and pilecap is 20.68 MPa (3000 psi). The laminated elastomeric bearing pad has internal steel plates in laminated pads according

to ASTM A-238, and has a dimension of $400 \times 600 \times 69$ mm. The detail of Shabqadqr Bridge is shown in Figure 2.

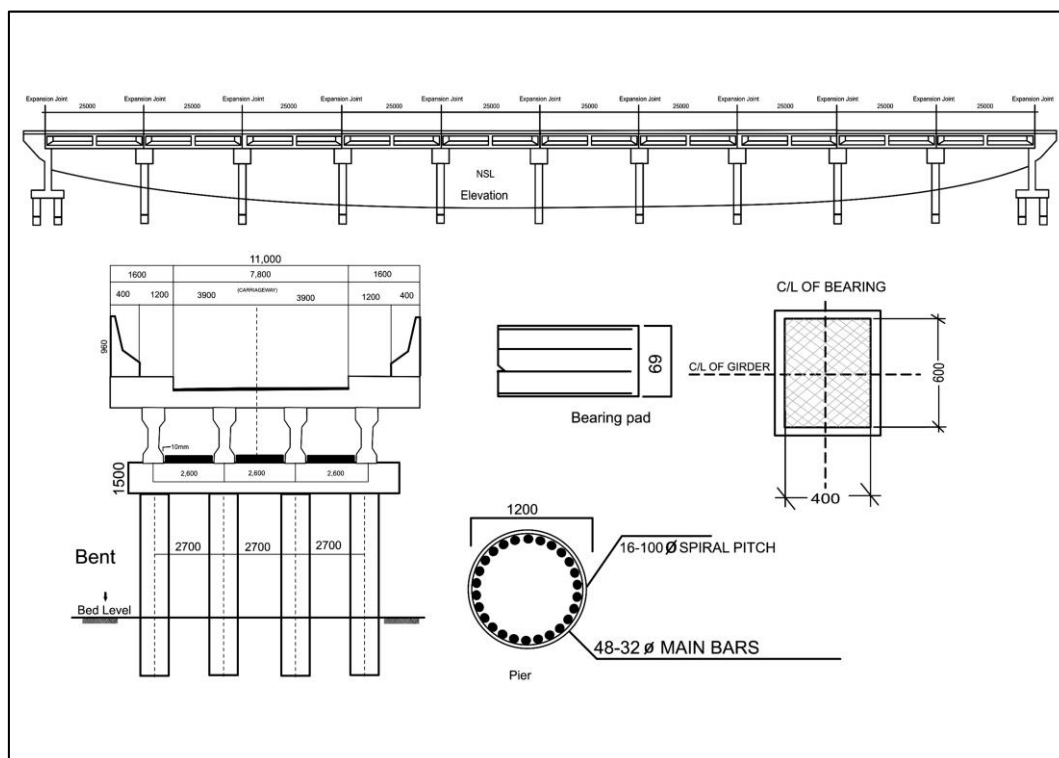


Figure 2. Shabqadar Bridge, Charsadda.

2.3. Dhoor Bridge Manshehra

The Dhoor Bridge is located in the district of Haripur in the province Khyber Pakhtunkhwa. It is a multi-span bridge with each span having the dimensions 30×100 mm, as shown in Figure 3 (layout plan drawings provided by “AA Associates” consultant firm). The superstructure consists of a post-tension girder holding deck slab. Four girders are rested on the elastomeric laminated bearing pad. They have nine intermediated bents with four solid circular pier shafts and rectangular transoms (cap beams) 2000×1200 mm. Every bent has a pile cap foundation. The bearing pad dimension is $500 \times 500 \times 82$ mm, and pad thickness is 82 mm. It has six 3 mm steel plates embedded in five 12 mm rubber plates and 2 mm at the ends. Three rectangular diaphragm beams are constructed to hold four girders in the transverse direction. Pier shafts have 1200 mm dia. There are four girders in each span, spaced 2500 mm throughout the bridge. Each pier shaft has a 1200 mm dia. The cap beam has a dimension of 1200×2070 mm. There is a 25 mm expansion joint between the deck slab, girders, and abutment wall. The bearing pad is placed on a concrete pad with the help of a special epoxy grout cement pad. A shear block on the top of each column bent and an abutment is also built to prevent the lateral load and gap of 10 mm between girder and shear block filled by polystyrene. The concrete used in prestressed girders have 34.47 MPa (5000 psi) cylinder compressive strength, and other members (deck slab, diaphragm, and pile) have 27.58 MPa (4000 psi). Moreover, the compressive strength of the railing post, kerb, plank, and pilecap is 20.68 MPa (3000 psi). The laminated elastomeric bearing pad has internal steel plates in laminated pads conforming to ASTM A-238. It has a dimension of $400 \times 500 \times 46$ mm, as shown in Figure 3.

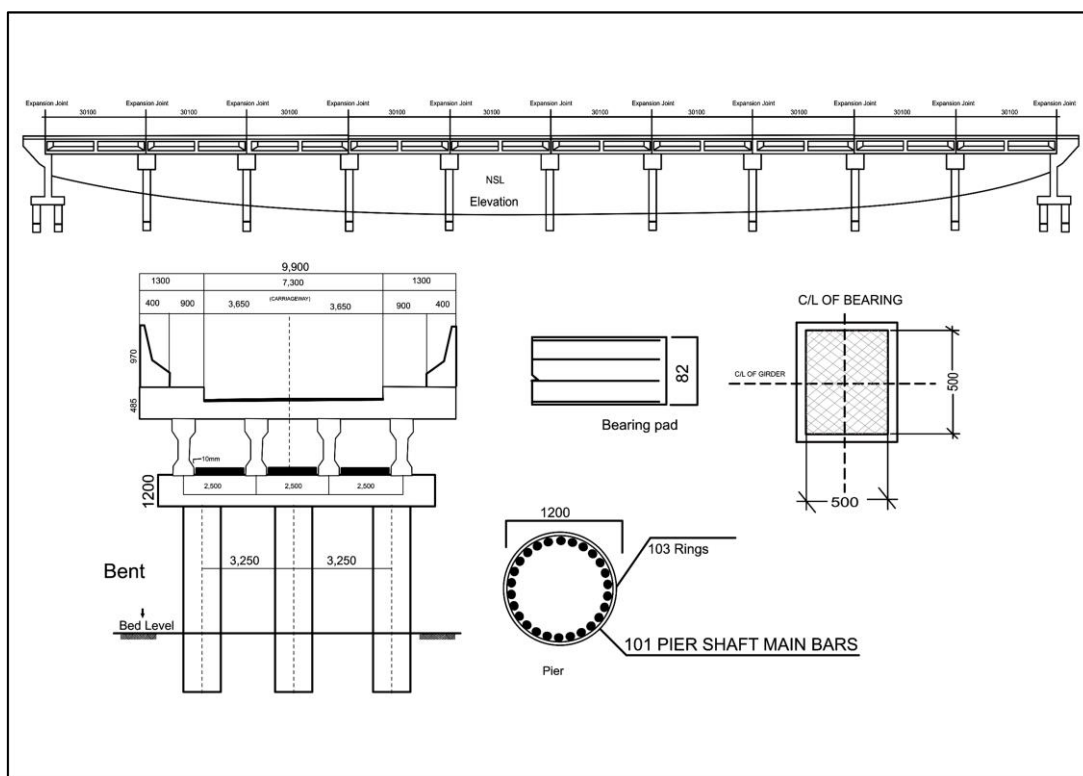


Figure 3. Dhoor Bridge, Mansehra.

The general properties of these three bridges are shown in Table 1.

Table 1. Properties of bridges.

Bridge ID	Bridge 1	Bridge 2	Bridge 3
Bridge name	Shabqadar	Dhoor	Mingora
No. of spans	10	10	3
Span length (mm)	10 × 25,000	10 × 30,100	3 × 16,100
Bridge width (mm)	11,000	9900	11,200
No. of girders	4	4	4
Girder material	Concrete	Concrete	Concrete
No. of piers	4	3	3
Pier diameter (mm)	D = 1200	D = 1200	D = 1200

3. Computational Models

Meshing is one of the significant components in the computational modeling of structures to find precise outcomes from an FEA numerical model. The elements in the meshing essentially take numerous aspects into account to discretize stress/ deformation gradients precisely. Characteristically, the lesser the extent of meshing, the more correct it will be across the real-time problems. The potential bottleneck of this simulation is that the more sophisticated the precision, the larger the simulations’ calculations become, and thus solve times are prolonged. There is no worth in outlaying additional hours simulating with a compact mesh if a coarser meshing will give us the desired outcomes. Researchers frequently accomplish convergence studies to achieve the optimum equilibrium between exactness and time. In this article, we carry out the parametric models of our bridge structures and find out in the convergence study of elements in mesh convergence corresponding to mid-span deflection of the bridge computational model, that increasing the mesh density beyond (1000) elements will not significantly diverge corresponding to deflection, therefore we limit of mesh element density to (1000) in order to optimize our result and reduce the computational time to solving numerical models as shown in Figure 4.

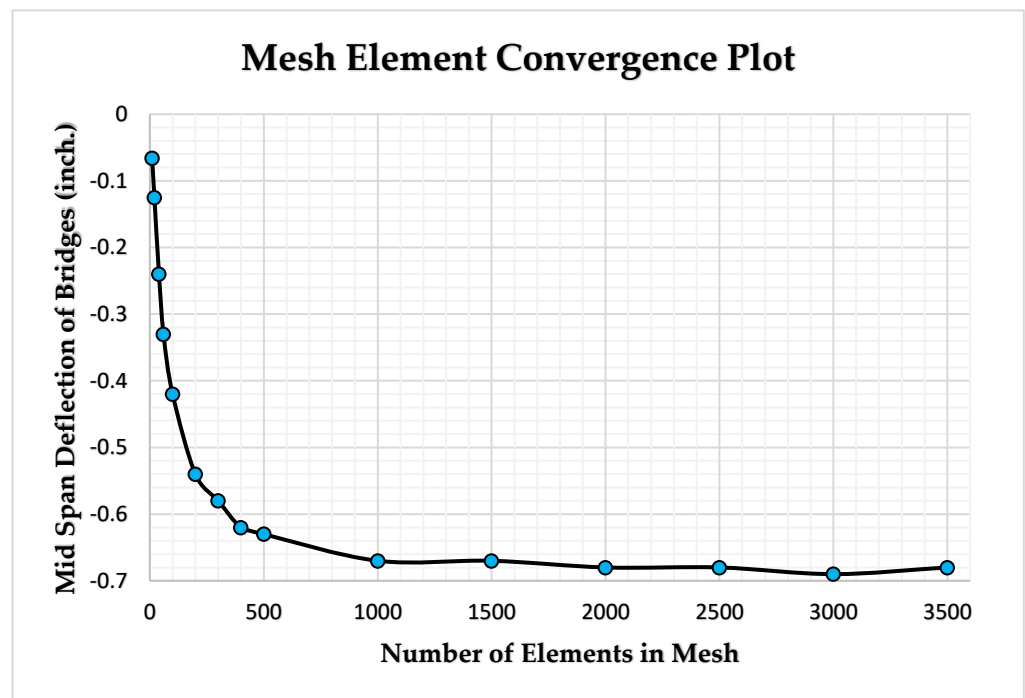


Figure 4. Mesh elements convergence plot.

Three-dimensional (3D) models are generated because they can capture the mass and geometric distributions of the structure. The axial load variation and pier response in the transverse direction is captured more accurately in 3D models [31]. Models of the bridges are generated in the finite element software package. Frame elements are used to generate the piers, girders, diaphragms, and cap beam components of the bridges. Link elements are used to generate the responses of the bearing pads and shear key [32]. Expansion joints are modeled with gap elements and deck slabs with shell elements. The piers, abutments, expansion joint, shear key, and bearing pads are non-linear components of the bridge, while the superstructure is a linear elastic component. Computational modeling of the Mingora, Shabqadar, and Dhoor bridges are shown in Figure 5a–c, respectively.

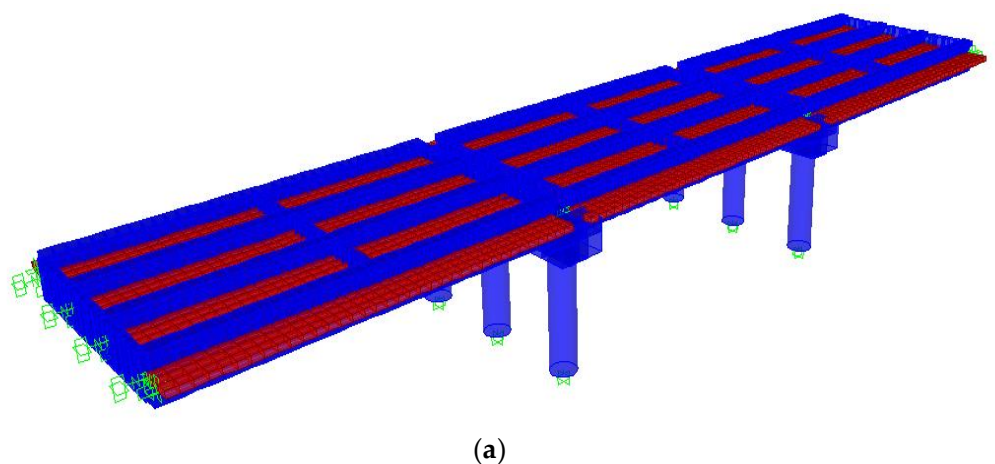


Figure 5. Cont.

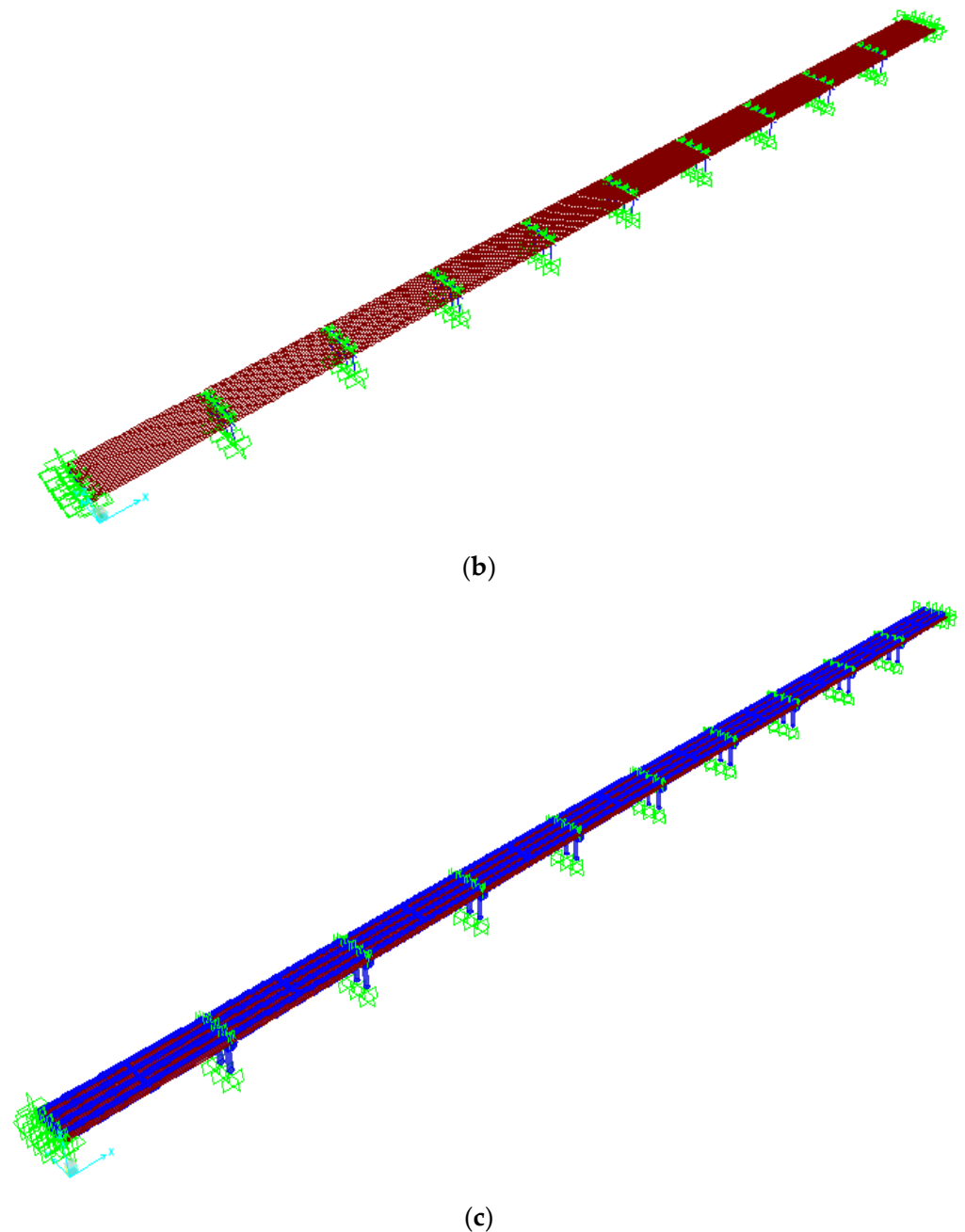


Figure 5. (a) FEM model of Mingora Bridge, Swat. (b) FEM model of Shabqadar Bridge, Charsadda. (c) FEM model of Dhoor Bridge, Mansehra.

3.1. Material Properties Modeling of Bridge

The ductile behavior of a plastic hinge is significantly affected by the non-linear material property used to define the frame member receiving the hinges. The material strength and stress–strain ($\sigma - \epsilon$) relation used for concrete was unconfined and confined using the Mander model and reinforcing the steel model to precisely capture the bridge's capacity and behavior. The properties of cement concrete conformed to Section 3.2 of SDC 2004 [33]. The Mander et al. (1988) [34] model represents the uniaxial stress–strain behavior of unconfined and confined concrete, as shown in Figure 6. The tensile stress is measured by ACI 318 as $f_r' = 0.6 \sqrt{f_c'}$ (MPa) for concrete having normal weight, with an initial modulus of elasticity E_c according to Section 3.2 of SDC 2004.

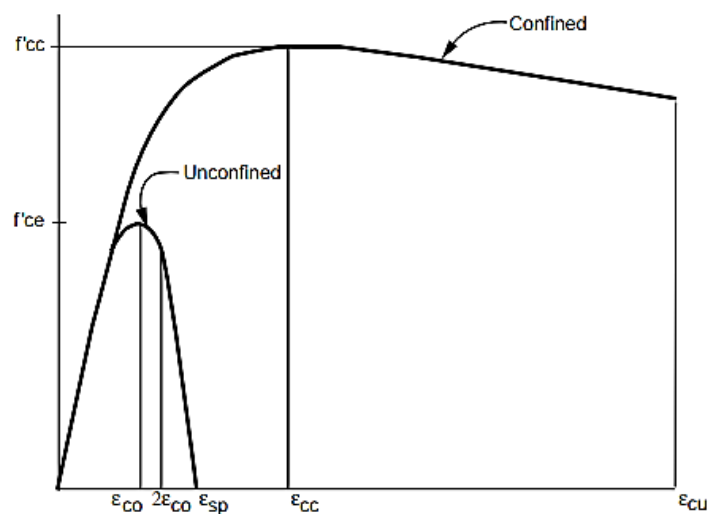


Figure 6. Concrete Mander (1988) stress–strain model.

A moment curvature ($M-\phi$) analysis is to be carried out for the concrete column (see Section 3.4.2); the steel longitudinal and transverse reinforcement properties are to be used according to Sections 3.2 and 3.2.2 of the SDC 2004 Guidelines for Steel ASTM A-706. The steel material model in tension and compression regions assumes an initial elastic behavior to yield strength rather than a yield strength, tracked by a strain-hardening section. According to SDC 2004, Section 3.2, the maximum expected values of yield stress (f_{ye}) and ultimate stress (f_{ue}) for all bar sizes are to be taken as 448 and 655 MPa, respectively, as shown in Figure 7.

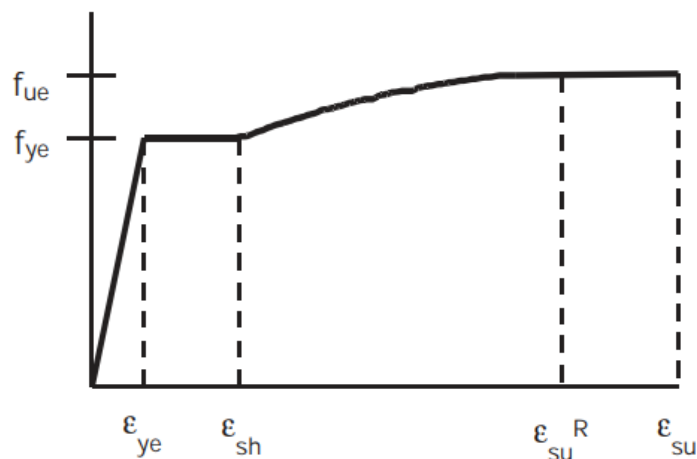
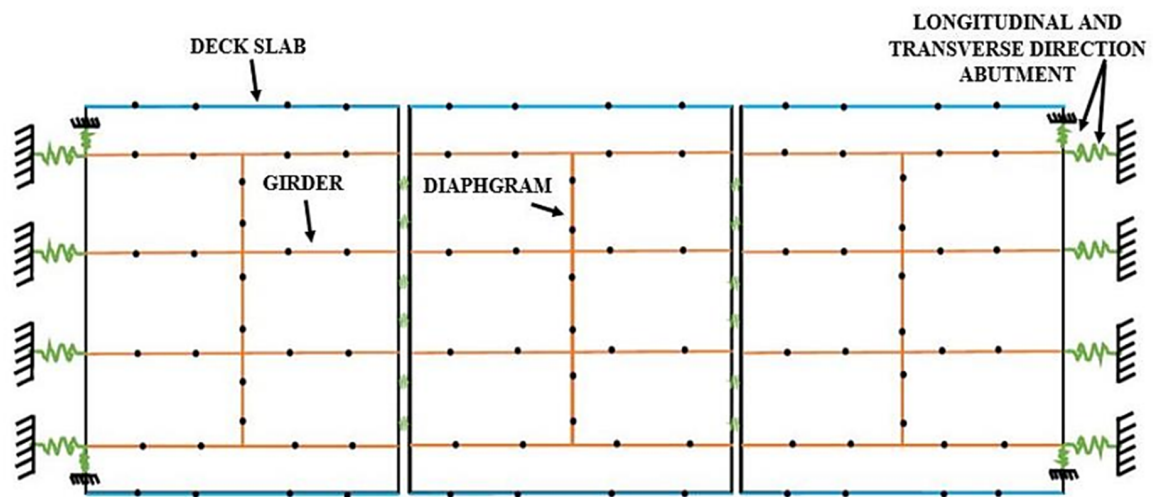


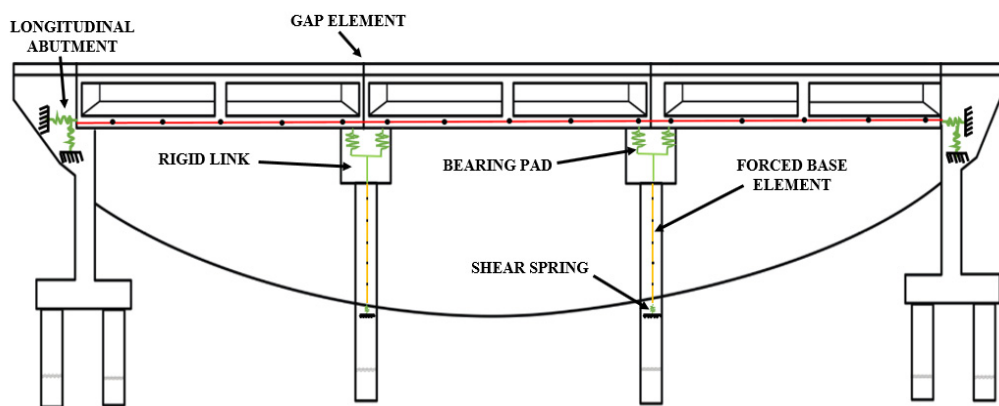
Figure 7. Steel stress–strain model.

3.2. Finite Element Modeling of Bridge

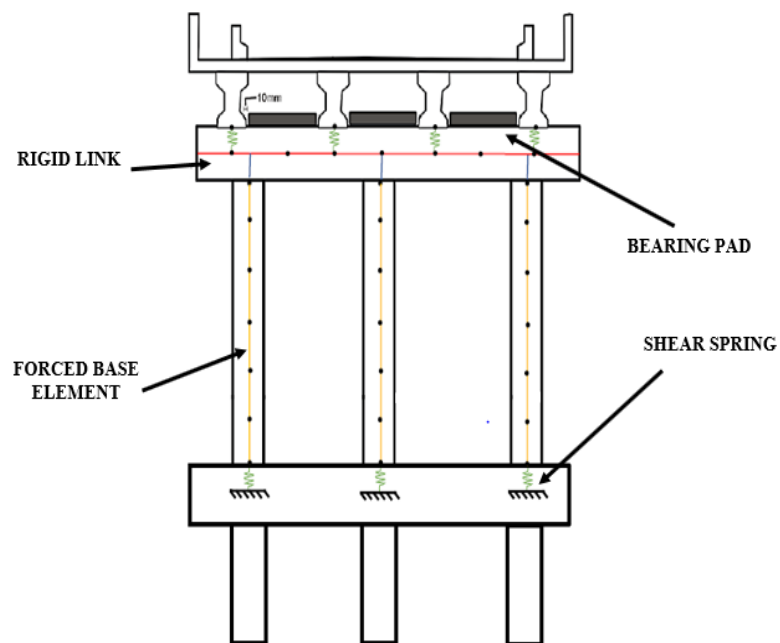
A numerical model of the bridges was developed in the finite element analysis program. The properties used in generating the models are listed in Table 1. The contact (constrain) properties are used for generating the computational model. For example, frames, girders, and piers etc. are modeled by a rigid link element. Shell elements were used to model the slab, while bi-linear link elements were used to model bearing pads and abutments. A gap element was used to model expansion joints. These numerical models of the bridges are shown in Figure 8a–c, respectively.



(a)



(b)



(c)

Figure 8. (a) FEM modeling of bridge deck. (b) FEM modeling of bridge (longitudinal section). (c) FEM modeling of bridge bent.

The characterization of the boundary/edge conditions in a structural arrangement is a significant feature in the accumulation of its stiffness matrix, thus affecting both the static and dynamic performance of the structural system. The boundary conditions must be allocated appropriately through simplified and realistic models of the bridge abutments and footing system to properly estimate the ductility capacity and seismic demand on key structural sections. In a dynamic analysis of the bridge, the modal periods and mode shapes, as well as other related properties, are greatly affected by such assignments. In this article, bridge footing is constrained by a fixed support system. Bridge abutment, bearing pad, and shear key ponding is discussed in detail in the later sections.

3.2.1. Bearing Pads

Bearing pads are modeled as link elements with non-linear constituent laws. There are two possible failure modes of the bearing pads: (1) failure in shear between the neoprene and steel reinforcement and (2) failure in sliding between the neoprene and contact surface of the overlaying girder. According to Tortolini and Annunzio, [35] shear failure force varies from 1.2 to 1.8 times G (shear modulus). The seismic design criteria (SDC) of the California State Department of Transportation CALTRANS-2006 [36] recommends the ratio between the normal (dead load) force and horizontal failure force (sliding force) acting on the bearing pad to be 0.40.

In this work, the sliding failure of the bearing is considered, and an elastoplastic force–displacement relationship is assumed for the bearing pads shown in Figure 9. Since the link element has six degrees of freedom, the rotational degree of freedom is assumed as zero. The translational stiffness values are calculated using the relationship given by Equation (1) proposed by [37]. Table 2 presents the properties of bridge-bearing pads.

$$K_h = G * \frac{A_b}{H} \quad (1)$$

where,

K_h = horizontal stiffness of the bearing pad G = shear modulus of neoprene rubber, A_b = area subjected to shear; and H = the total thickness of the pad excluding steel plates. In the vertical direction, the stiffness is assumed as 100 times K_h , shown by Equation (2) as follows:

$$K_v = G * K_h \quad (2)$$

where K_v = horizontal stiffness of the bearing pad, and G = shear modulus considered 1 MPa.

Mathematically shear failure force and shear stress in the bearing pad is expressed by Equations (3) and (4) as follows:

$$V_f = \tau * A_b \quad (3)$$

$$\tau = (1.2 - 1.8) * G \quad (4)$$

where V_f = shearing failures subjected to the area of bearing A_b , and τ = shearing stress.

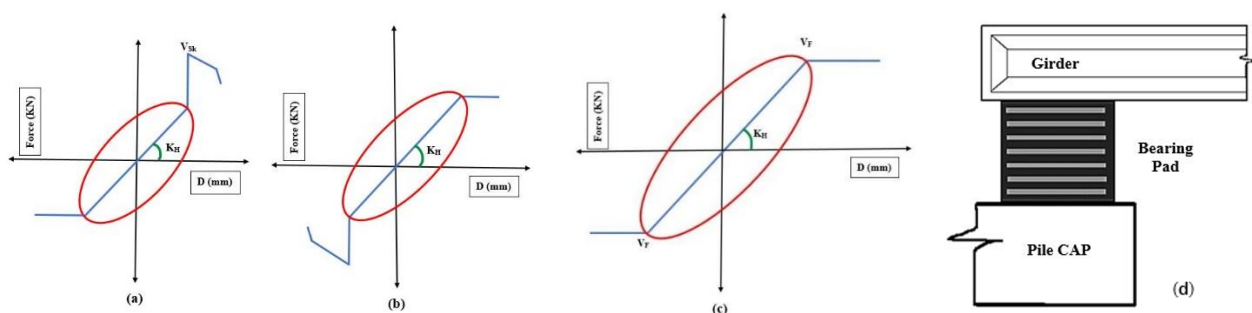


Figure 9. (a,b) F–D relation in transverse direction and in (c) longitudinal direction, (d) Bearing pad modeling.

Table 2. Properties of bridge's bearing pads.

Sr. #	Bridge Name	Spans	Bearing Pad Area (Ab, mm)	Neoprene Thickness (H, mm)	Horizontal Stiffness (K _h , kN/mm)
1.	Charsadda Bridge	10	400 × 600	69	4706
2.	Dhoor Bridge	10	500 × 500	82	3906.3
3.	Mingora Bridge	03	400 × 550	38	5789

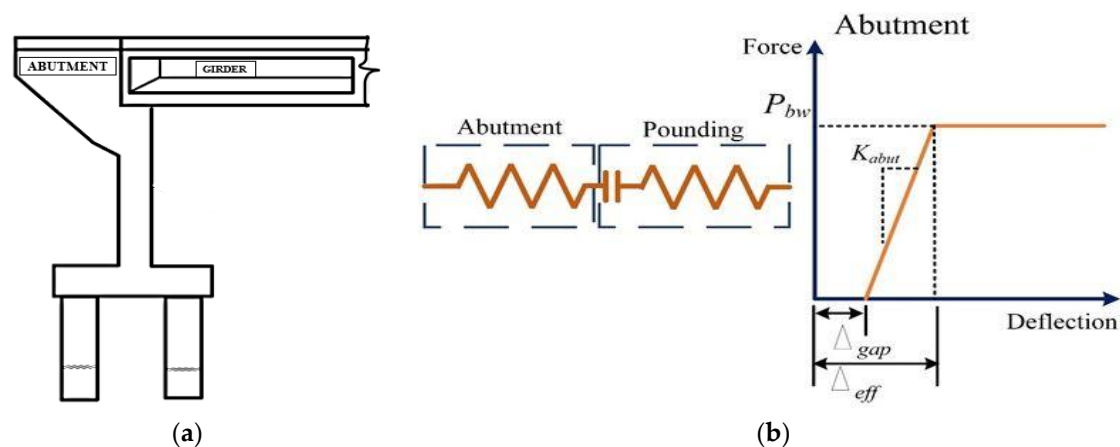
3.2.2. Abutments

The abutments of all three bridges are seating abutments, and they are considered the non-linear component of the bridge. Their force–displacement relationship is modeled as elastic, perfectly plastic based on the recommendations of Caltrans (2006) [36] as shown in Figure 10a,b. Caltrans proposed the maximum passive pressure (P_{bw}) given by Equation (5). The stiffness of the abutment is computed by Equation (6). K_i is the initial stiffness, and its value is taken based on the test of large-scale abutment carried out at the University of California Davis (i.e., 20 kips/in/ft. or 11.5 kN/mm/m proportioned to the height of the back wall) [38].

$$P_{bw} = A_e * 239(\text{Kpa}) * h_{bw}/1.7 \quad (5)$$

$$K_{abut} = K_i * W * h/1.7 \quad (6)$$

W = The back wall/diaphragm width for seat and diaphragm abutment, K_i = the initial stiffness value.

**Figure 10.** (a) Abutment modeling. (b) abutment modeling F–D relation.

3.3. Expansion Joint

A gap, ponding, or expansion joint can alter the response of a bridge in a seismic event. We can model in (Sap2000) by connecting link elements by a linear or bilinear spring model as shown in Figure 11a,b. It is challenging to depict the exact behavior of these springs. Susender et.al [39] observed at the bridge's gap and device a method to model it by a stereo mechanical method; during shaking and drift, seismic energy is dissipated and expressed in Equation (7).

$$\Delta E = \frac{Kh\delta_m^{n+1}(1 - e^2)}{n + 1} \quad (7)$$

where “ ΔE ” = the dissipation of energy, “ Kh ” = an impact stiffness as $868.675 \text{ kN}\cdot\text{mm}^{-3/2}$, “ n ” = the hertz (as valued $3/2$), “ e ” = restitution-coefficient valued “ $0.6\text{--}0.8$ ”, and “ δ_m ” = max. penetration of the adjacent bridge slab. Linear models are suggested for equal dissipation of energy as yielded. Our first priority is to control the penetration “ δ_m ” max. value. “The effective stiffness” (K_{eff}), as shown in Figure 11b. is computed as:

$$K_{eff} = Kh\sqrt{\delta m} \tag{8}$$

where study shows the max. “ δm ” is presumed to be “1 in”, “ K_{eff} ” as 182,306.9 kN/m (1041 kip/in) [38].

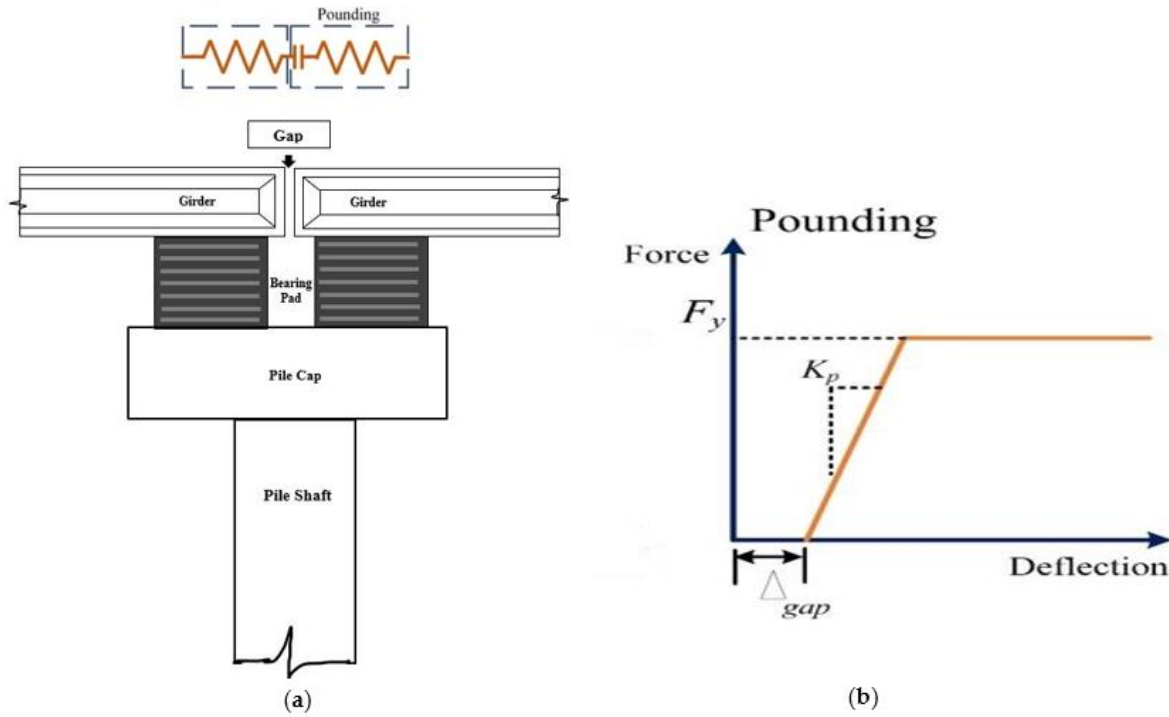


Figure 11. (a) Expansion joint. (b) Expansion joint F–D relation.

3.4. Plastic Hinges, Performance Limit and Bridge Piers

The lump plasticity approach is been carried out in this research. Plastic hinges are assigned to piers of bridges. These hinges are provided at the top and bottom of every pier. Hinge lengths (L_p) are computed by Equation (9) given in (Caltrans SDC, 2013) [40].

$$L_p = 0.08L + 0.022 f_{y e} d_{b l} \geq 0.044 f_{y e} d_{b l} \text{ (mm, MPa)} \tag{9}$$

where, L is the pier; $f_{y e}$ denotes the expected yield strength of longitudinal reinforcement, and ‘ $d_{b l}$ ’ represents the nominal bar diameter of longitudinal reinforcement. Plastic hinges are assigned at the mid-height of the plastic zone with a segmental length $L = L_p$ as shown in Figure 12.

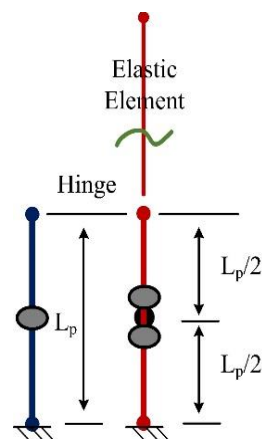


Figure 12. Computation of hinge length.

The plastic hinge's rotation directs the capacity of a member to endure inelastic distortion and is used in SAP000 to define column plastic hinge properties. (FEMA-356, 2000) provides a generalized F–D relation model shown in Figure 13 for the static non-linear analysis procedure, and the auto model in SAP2000 (PMM hinge in SAP2000) for the axial load moment hinge.

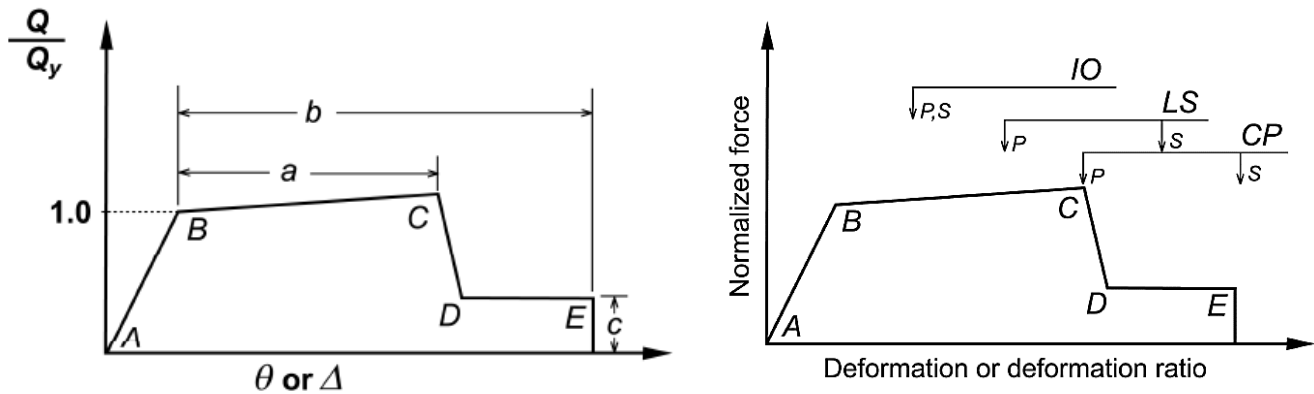


Figure 13. Force deformation relation (back bone curve) of plastic hinge.

Elastic behavior from initial position “A” to significant yielding point “B” defines the F–D curve. At that point, the stiffness cut from point “B” to “C”. “C” point has a confrontation equal to the nominal strength, then an abrupt lessening in the cross-load resistance to the retort at reduced resistance “D” to final loss of resistance “E”. The slope of “BC” is generally achieved in “0 and 10%” of the initial condition. The “CD” slope links to the preliminary failure of the section. The “DE” slope depicts the remaining strength of the section. These slopes are referred to (FEMA-356, 2000) in order to limit the “hinge rotation” behavior of RC Sections. The slope lines “B” and “C” represent acceptance criteria for the hinges rotation, which is referred to as immediate occupancy (IO), life safety (LS), and collapse prevention (CP) [41].

3.4.1. Performance Limits

Two categories generally define performance limits or acceptance criteria: (i) global structural performance limits and (ii) local member/elements level performance limits. (FEMA-356, 2000) [26,27]. The global-level acceptance criteria depict the capacity of the structure to endure gravity and lateral loading. The lateral load capacity of structural performance should not be degraded by 20% of its overall strength. Lateral displacements should verify against standard limits (ATC-40, 1996) as given in Table 3.

Table 3. Deformation limits for each performance level (ATC-40).

Immediate Occupancy	Damage Control	Life Safety	Structural Stability
0.01	0.01–0.02	0.02	0.33 V_i/P_i

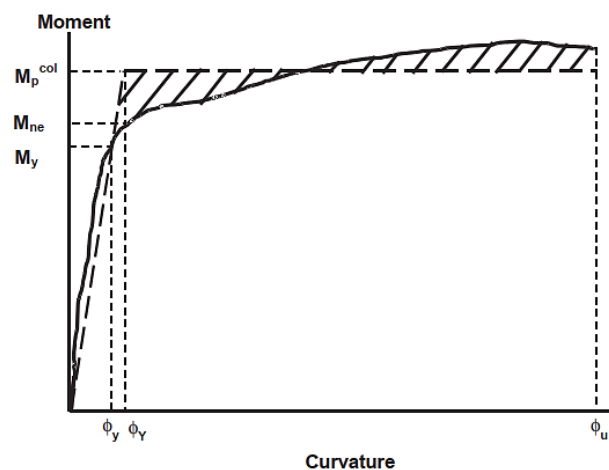
The local member/elements level performance limits are often imposed by nonstructural and component damage in structural elements, such as beams and columns. They are constructed on the plastic hinge rotation capacities limit. Table 4, below, states the “deformation limits” referred to by (ATC-40, 1996). Hence, cross-verification of the failure of elements by “flexural demands” and “shear failure” does not befall earlier than these rotation limits are reached.

Table 4. Plastic rotation limits for RC column controlled by flexure (ATC-40).

$\frac{P}{Agf_c}$	Trans. Reinf.	$\frac{V}{bw d\sqrt{f_c}}$	Modeling Parameter			Plastic Rotation Limit		
			a	b	c	Immediate Occupancy	Life Safety	Structural Stability
≤ 0.1	C	≤ 3	0.02	0.03	0.2	0.005	0.001	0.020
≤ 0.1	C	≥ 6	0.016	0.024	0.2	0.005	0.001	0.015
≥ 0.4	C	≤ 3	0.015	0.025	0.2	0.003	0.005	0.015
≥ 0.4	C	≥ 6	0.012	0.02	0.2	0.003	0.005	0.010

3.4.2. Moment Curvature of Bridge Piers

The capacity of all ductile concrete structure sections for non-linear plastic hinge/plastic moments shall be considered by $M-\phi$ plot dependent on anticipated material properties. $M-\phi$ plot derives the curvatures linked with a range of moments for an x-section depending on the principles of strain considerations and balance of forces. The moment curvature ($M-\phi$) plot can be idealized (bi-linearization) with an elastic, perfectly plastic response to approximate the plastic moment capacity of a member's x-section. The elastic region of the idealized (bi-linear) curve must pass through the point, indicating the first reinforcing bar yield. The idealized plastic moment capacity is attained by corresponding to the areas between the actual and the idealized $M-\phi$ plots beyond the first reinforcing bar yield point, as shown in Figure 14.

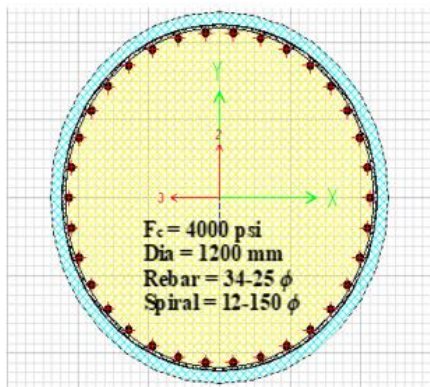
**Figure 14.** Moment curvature curve.

Moment curvature analysis for piers is designed and analyzed in SAP2000 as shown in Figures 15–17; maximum axial dead load is carried out to examine the yield moment and consider the yield and ultimate curvature rotation for the three bridges, and in Equations (10)–(12), these parameters are stated for the Mingora, Shabqadar, and Dhoor Bridges, respectively.

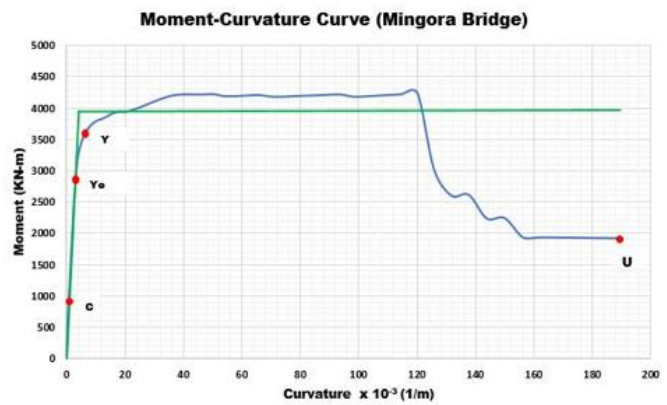
$$\begin{aligned} M_y &= 2737.41 \text{ kN-m;} \\ \phi_y &= 0.00284 \text{ (1/m); } \phi_u = 0.1696 \text{ (1/m);} \\ P &= 1345 \text{ kN} \end{aligned} \quad (10)$$

$$\begin{aligned} M_y &= 5151.482 \text{ kN-m;} \\ \phi_y &= 0.00314 \text{ (1/m); } \phi_u = 0.171 \text{ (1/m);} \\ P &= 1468 \text{ kN} \end{aligned} \quad (11)$$

$$\begin{aligned} M_y &= 2759.458 \text{ kN-m;} \\ \phi_y &= 0.00288 \text{ (1/m); } \phi_u = 0.1706 \text{ (1/m);} \\ P &= 1453 \text{ kN} \end{aligned} \quad (12)$$

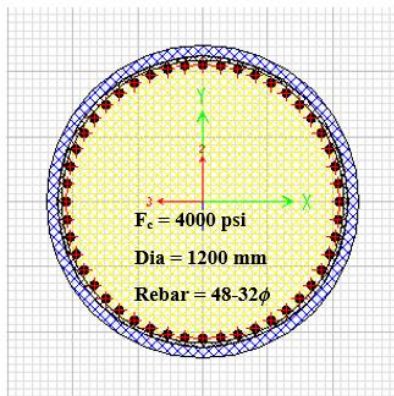


(a)

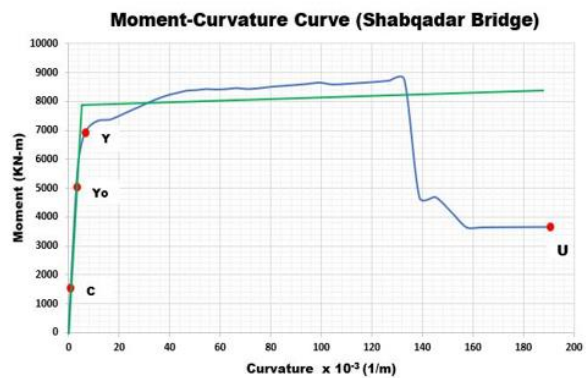


(b)

Figure 15. (a) Cross-sectional detail of Mingora Bridge. (b) Moment curvature of Mingora Bridge.

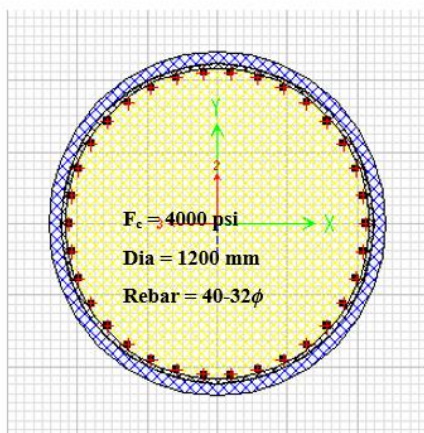


(a)

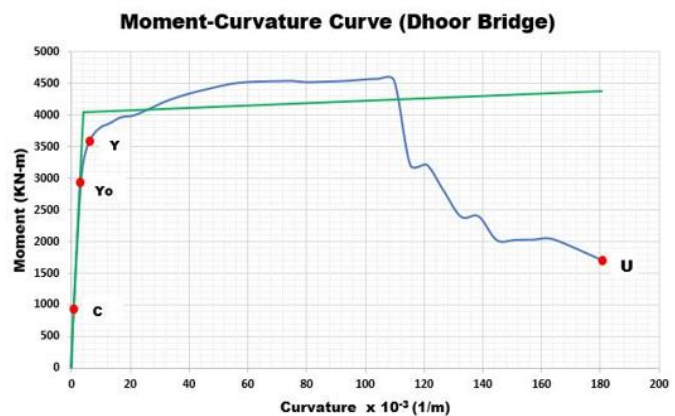


(b)

Figure 16. (a) Cross-sectional detail of Shabqadar Bridge. (b) Moment curvature of Shabqadar Bridge.



(a)



(b)

Figure 17. (a) Cross-sectional detail of Dhoor Bridge. (b) Moment curvature of Mingora Bridge.

4. Response Modification Factor (R-Factor)

The main objective of earthquake-resistant design is: (1) In the event of minor earthquakes (less damaging), the structural response is in the elastic region. (2) In case of a significant earthquake, the structure can resist and sustain the overall stability. In major earthquake events, structures respond in the non-linear range. Therefore, non-linear analysis is required to describe the behavior of structures. However, due to the simple elastic procedures, traditional analysis procedures are based on linear analysis suggesting the reduced seismic forces. The schematic base shear-displacement response of a traditional structure is shown in Figure 18.

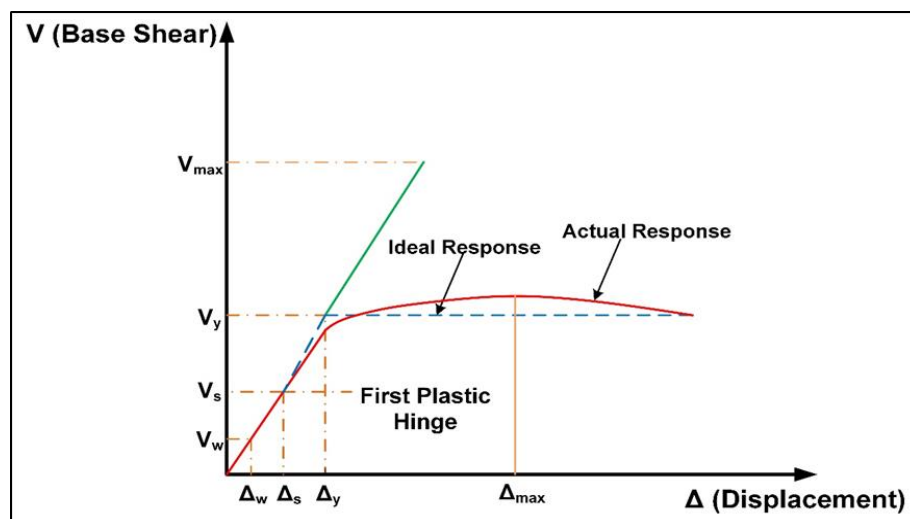


Figure 18. Computation of R-Factor.

The response modification factor (R) is a significant feature in building seismic design. Equivalent statistical analysis (ESA), which is recurrently used to evaluate the seismic response of structures, can be executed by shaping the R -factor. In actuality, R -factor directs the capacity of a structure to dissipate energy in an inelastic manner [42,43].

As mentioned before, R -factor is a significant parameter in designing vulnerable seismic design. During an earthquake event, it considers the level of inelastic behavior of the structure. R -factor is defined by (NEHRP 1988) [44] as the “factor intended to account for both damping and ductility inherent in structural systems at the displacements great enough to approach the maximum displacement of the systems” [44]. This definition delivers an intuition into the consideration of the seismic behaviors of the structure and the predictable response of code-based structures in the design earthquake. R -factor decreases the design forces in seismic resilient structures based on the damping, energy dissipation capacity, and overstrength of the structure [45].

This reduced seismic force is extracted by dividing the elastic base shear by (R -factor). In another sense, in the linear analysis [27], the elastic base shear force level (V_e), is reduced to the force level corresponding to the appearance of the first plastic hinge in the structure (V_s).

4.1. Uang’s Procedure R-Factor Coefficient Method

Uang’s procedure [30] is one of the methods used to compute the R -factor. The extreme base shear is considered when the structure remains in the elastic zone. The R -factor comprises a reduction factor due to ductility (R_μ) and an overstrength coefficient (Ω). R_μ is the proportion of base shear at the elastic level (V_e/V_{max}) and to the base shear at the level of structural failure (V_y); and Ω is definite as the fraction of the base shear at strength level, which corresponds to the formation of a yield mechanism (V_y) to the base shear of the structure when the primary plastic hinge is formed (V_s). Conferring to Figure 16, the mandatory elastic resistance due to the base shear coefficient is determined by Equation (13).

$$C_e = \frac{V_e/V_{\max}}{W} \quad (13)$$

where, W is the effective structural weight, and V_e is the maximum base shear when the structure is in the elastic range. Regarding the Uang's method, the required equations for calculating R-factor are as follows:

$$\Omega = \frac{V_y}{V_s} \quad (14)$$

$$R_\mu = \frac{V_e/V_{\max}}{V_y} \quad (15)$$

$$R = \frac{V_e/V_{\max}}{V_s} \times \frac{V_y}{V_s} = R_\mu \cdot \Omega \quad (16)$$

The structure ductility, μ , is defined in terms of the maximum structural drift (Δ_{\max}) and the displacement corresponding to the idealized yield strength (Δ_y) as in Equation (17):

$$\mu = \frac{\Delta_{\max}}{\Delta_y} \quad (17)$$

Many researchers have deliberated the two key components of R-factor presented in Equation (16). The ductility-dependent component, R_μ , has received substantial consideration. Ductility reduction factor R_μ is a function of the structure's features, including ductility, damping, fundamental period of vibration (T), and the features of earthquake ground motion [46], which presented a relation for R_μ in the following form:

$$R_\mu = [c(\mu - 1) + 1]^{1/c} \quad (18)$$

where

$$c(T, \alpha) = \frac{T^a}{1 + T^a} + \frac{b}{T} \quad (19)$$

In Equation (19), α is the post-yield stiffness given as a percentage of the initial stiffness of the system, and a and b are parameters given as functions of α that can be obtained from Table 5 [46]. Alternatively, we can also attain " R_μ " corresponding to "time period" by help of the chart as shown in Figure 19, which is proposed by Nassar and Krawinkler [47] instead of using Equation (18).

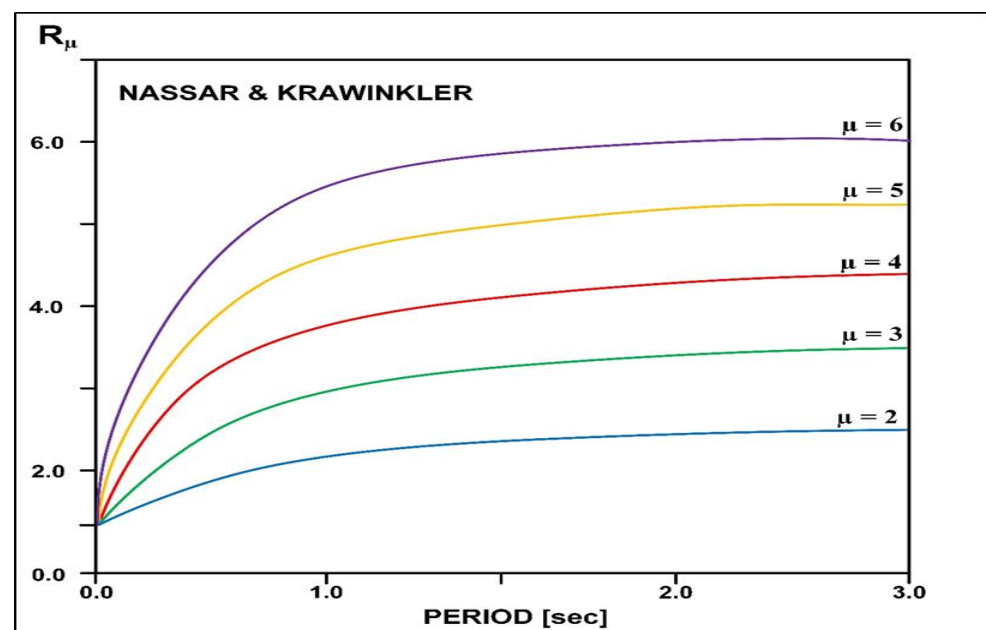


Figure 19. Strength reduction factor proposed by Nassar and Krawinkler.

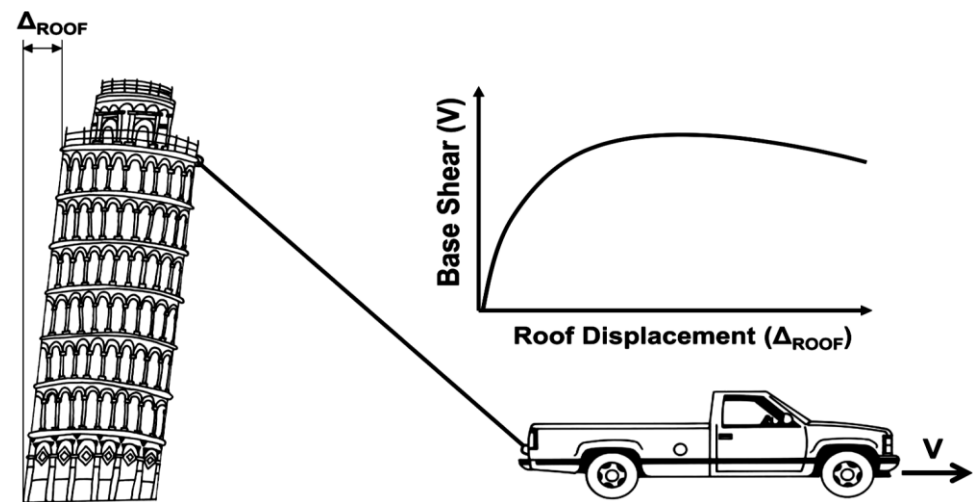
Table 5. Values regarding α .

α (%)	a	b
0	1	0.42
2	1	0.37
10	0.8	0.29

4.2. Nonlinear Static Pushover Analysis (NLSPA)

Pushover analysis is a very popular technique used for seismic assessment of the structure. In this procedure, a gravity load is applied to the structure and a load vector is applied sideways, and the structure is pushed until an ultimate limit is reached. The fundamental output of pushover analysis is a force versus displacement curves, also known as the capacity curve. Capacity curves provide information about the ductility and strength capacity of structures. In this work, the displacement coefficient method pushover analysis documented in (FEMA-356, 2000) [48], is used.

The non-linear static procedure (NLSP) is considered as just an analog of the linear static procedure (LSP) (i.e., that the static later loading is imposed on non-linear models of the structure). The monotonic pushover analysis (POA) is the most important tool of all present nonlinear static procedures (NSP). The primary working principle of pushover analysis (POA) is that after applying a gravity load on the non-linear model of the considered structure, the lateral load pattern (simple distribution of seismic forces) is applied, as shown in Figure 20. This procedure progresses until that structure becomes unstable or deteriorated, or the pre-assumed targeted deformation is touched [49].

**Figure 20.** Idealized concept of pushover analysis (POA).

The key objective of pushover analysis (POA) is to evaluate overall lateral strength, deformation ductility, and the deterioration mechanism of the considered structure with the influences of seismically induced lateral forces on the structure. At the global structural level, the monotonic/pushover or (capacity curve) of the detailed numerical structure model straightaway comprises the predicted nonlinearity of structural members. The maximum seismic displacement and other induced parameters can be obtained via any recognized non-linear static procedure. Then, these pushover curves are idealized (bilinear relation) in any simple form or relation for analysis simplicity. Comparing both linear static procedure (LSP) and nonlinear static procedure (NSP), the latter advances over the former procedure based on its ability to redistribute the elemental internal forces of the structure that constantly undergo incremental seismic lateral loads. This created a vivid understanding of how structures respond inelastically and achieved several limit states when undergoing an inelastic zone. The existing non-linear static procedure (NLSP) is designed on the principle of a detailed structural model of structures converted into an

idealized single degree of freedom system (SDOF). The global structure response of the pushover curve can be idealized in such a manner that it depicts the nonlinear force–displacement ($F-\Delta$) relation. This force–displacement ($F-\Delta$) relation is assigned to the idealized (SDOF), which is then predicted to behave as an actual non-linear detailed structural model. This procedure is explained in detail in Figure 21 [49].

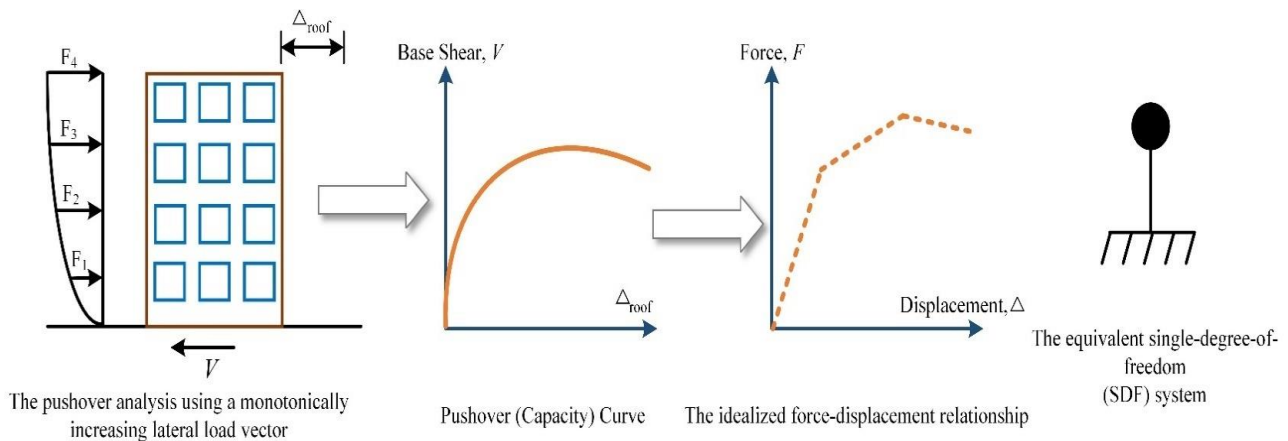


Figure 21. Broader concept of pushover analysis (POA).

4.2.1. The Capacity Spectrum Method (CSM)

The primary nonlinear static procedure (NSP) given in the ATC 40 (1996) [50] report entitled “seismic evaluation and retrofit of concrete buildings”, is working on the equivalent linearization approach (the capacity spectrum method, CSM), which was first advanced as a rapid evaluation method for a pilot seismic risk project of the “Puget Sound naval shipyard for the U.S. navy in the early 1970s” [49]. In this procedure, the capacity or (NSP) curve is changed into the “capacity spectrum” using point-by-point alteration of the coordinates of the modal spectrum. The first-mode inertia load vector generates this pushover curve. The base shear (V_b) and roof displacement (Δ_{roof}) of the capacity curves are transformed into the conforming spectral acceleration (S_{ai}) and spectral displacement (S_{di}) values on the capacity spectrum using the Equations (20) and (21).

$$S_{ai} = \frac{V_b}{w/\alpha_1} \quad (20)$$

$$S_{di} = \frac{\Delta_{\text{roof}}}{PF1\phi_{1,\text{roof}}} \quad (21)$$

where W presented “seismic weight” (i.e., the sum of dead load and the likely live loads), α_1 and $PF1$ are the “modal mass coefficient” and “the modal participation factor for the first vibration mode respectively”, and $\phi_{1,\text{roof}}$ is “the roof level amplitude of the first vibration mode shape”. Every point on a capacity spectrum curve is associated with a unique spectral acceleration (S_a), spectral velocity (S_v), spectral displacement (S_d), and natural period (T). This reduced response spectrum is also converted to the acceleration–displacement response spectrum (ADRS) format using Equation (22).

$$S_d = \frac{T^2}{4\pi^2} S_a(g) \quad (22)$$

The modified response spectrum in the ADRS format is called the “demand spectrum”. This demand spectrum is overlaid with the capacity spectrum to find their intersection point, which corresponds to a condition for which the seismic capacity is equal to the demand imposed on the structure. This point is called the “performance point”, which estimates the actual maximum displacement expected during an anticipated earthquake. The overall procedure is shown in Figure 22.

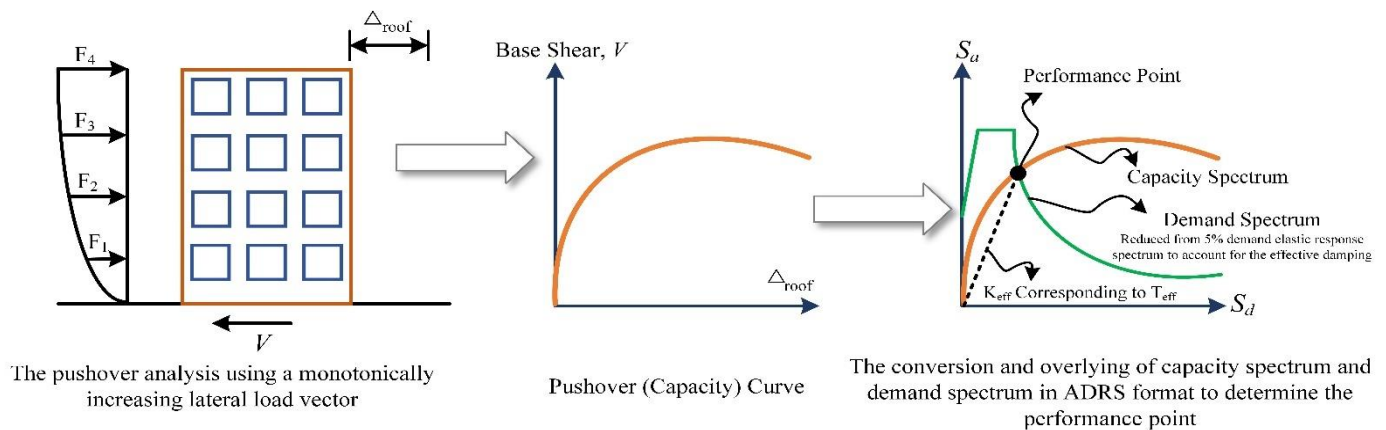


Figure 22. Capacity spectrum method (CSM) of pushover analysis (POA).

4.2.2. Displacement Coefficient Method (DCM)

This procedure uses the co-efficient to convert displacement of the linear to displacement of the non-linear system. This method is adopted by various codes, e.g., FEMA 356 [48], (FEMA-440) [51], and EC8. Figure 23 provides information about this procedure.

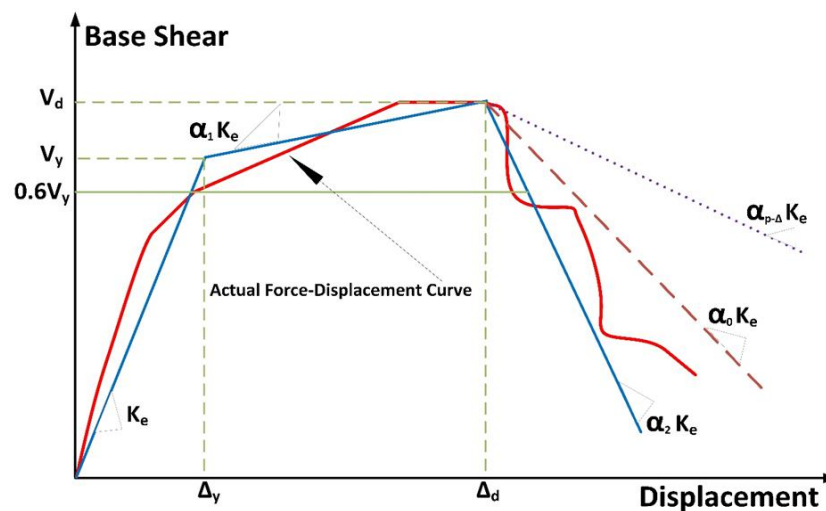


Figure 23. Displacement coefficient method (DCM) of pushover analysis (POA).

This method is carried by modifying the elastic response from the SDOF equivalent with coefficient factors C_0 , C_1 , C_2 , and C_3 [48].

$$\delta T = C_0 \cdot C_1 \cdot C_2 \cdot C_3 \cdot S_a \cdot \left(\frac{T_e}{2\pi}\right)^2 \cdot g \quad (23)$$

where, T_e is the effective fundamental period, C_0 is the modification factor for the spectral displacement of an equivalent SDOF system to an MDOF system, C_1 is the modification factor to relate the expected maximum inelastic displacement to the displacement calculated for the linear elastic response, C_2 is the modification factor that represents the effect of pinched hysteretic shape, stiffness degradation, and strength deterioration on the maximum displacement response, C_3 is the modification factor that represents increased displacement due to dynamic $P-\delta$ effect. S_a is the response spectrum acceleration in g (i.e., acceleration of gravity). Figure 24 shows the performance point according to the displacement coefficient method [41].

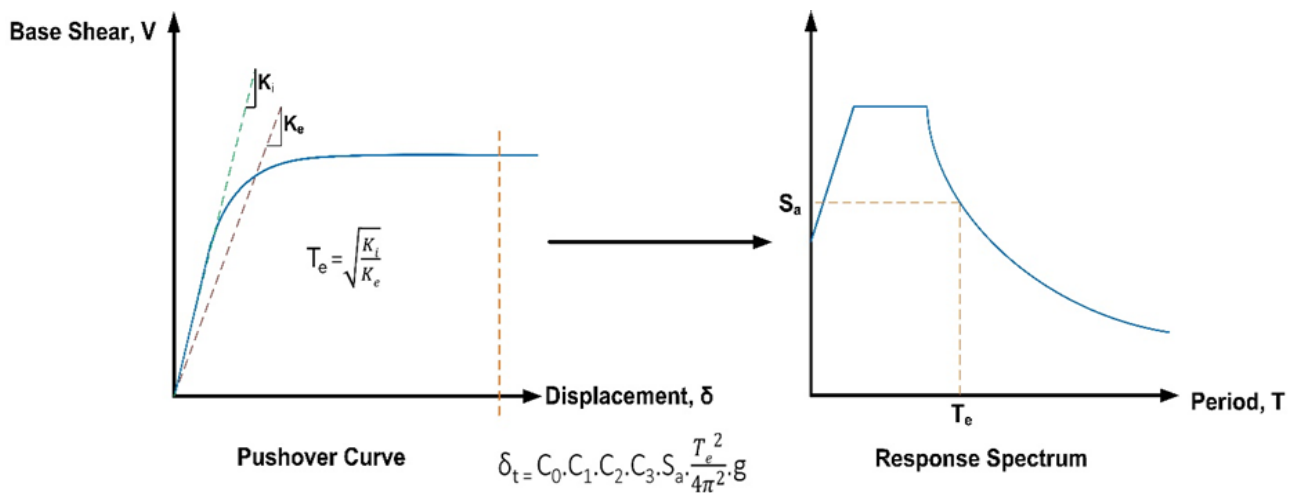


Figure 24. Coefficient method and target displacement DCM of pushover analysis (POA).

The first step is to determine the target displacement (δT). The procedure starts by setting an effective fundamental period that considers inelastic conditions. The effective fundamental period represents the linear stiffness of the equivalent SDOF system and corresponds to maximum spectral acceleration (S_d). Then, target displacement can be specified using Equation (23).

4.3. Response-Factor Computation

A block diagram of the process for computing the bridge models' R-factors is depicted in Figure 25. The capacity curves obtained by the pushover analysis depicted in Figure 23 and the parameters depicted in Figure 18 are used to find V_e , V_y , and V_s . Based on the elastomeric bearing pad parameters in Table 2, non-linear static analyses performed on the bridge models with the ERB isolator are also computed. The response modification factor is obtained by displacement coefficient method (DCM).

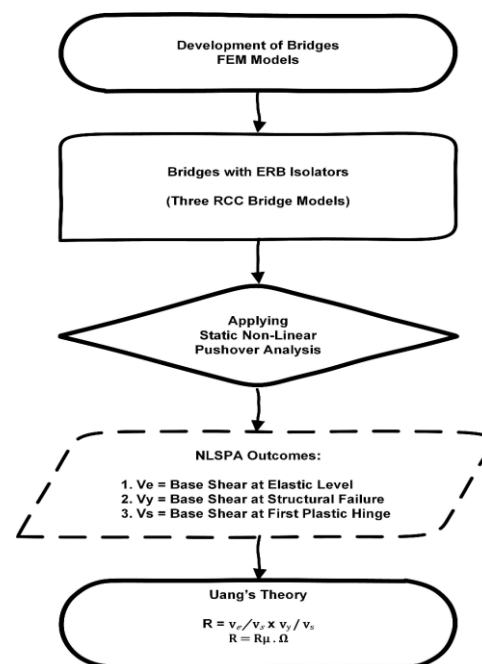


Figure 25. Flow chart for computing R-factor.

To evaluate the force reduction factors of concrete bridges at the ultimate limit state, three bridges that cross the three regions of the KPK province of Pakistan, Mingora, Shabqadar, and Thrace, were selected. The basic characteristics considered in the classification are the type of deck, type of piers, and type of pier-to-deck connections, as mentioned in Table 1. All three of the selected structures belong to the category defined in the previous Section 2, which is a deck supported through elastomeric bearings on elastically responding piers. The selected bridge's main features are given in Figure 1, Figure 2, and Figure 4. The pushover curves derived using analysis with SAP-2000 point hinge models (lumped plasticity), as mentioned in the previous Section 3, were idealized as bilinear curves (Figures 26–31) to define a conventional yield displacement (d_y) and ultimate displacement (d_u) by the method mentioned in a previous Section 4.2.2. The derived overstrength factors for bridges with yielding piers and the ductility factors for the same bridges are given in Tables 6–11.

Mingora Bridge Capacity Curve In Transverse Direction

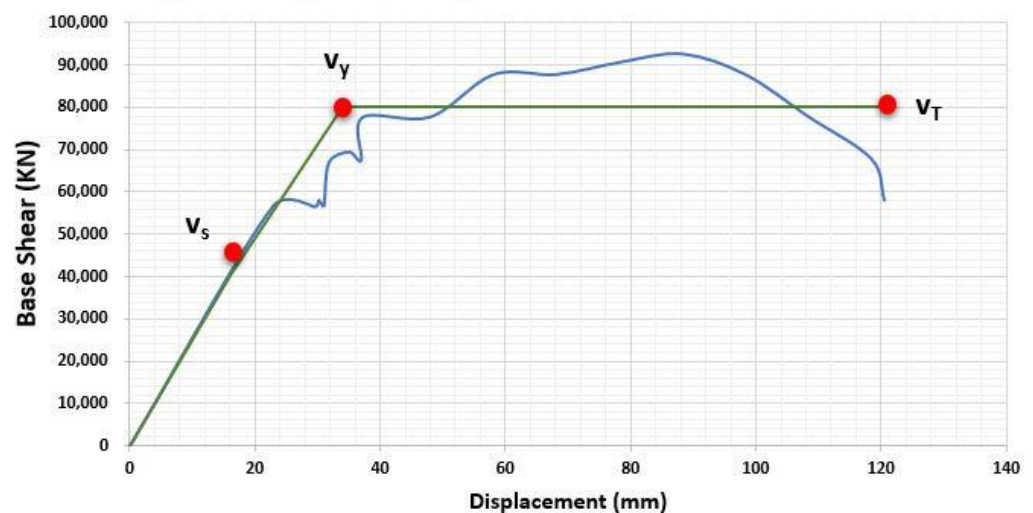


Figure 26. Mingora Bridge R-factor in transverse direction.

Mingora Bridge Capacity Curve In Longitudinal Direction

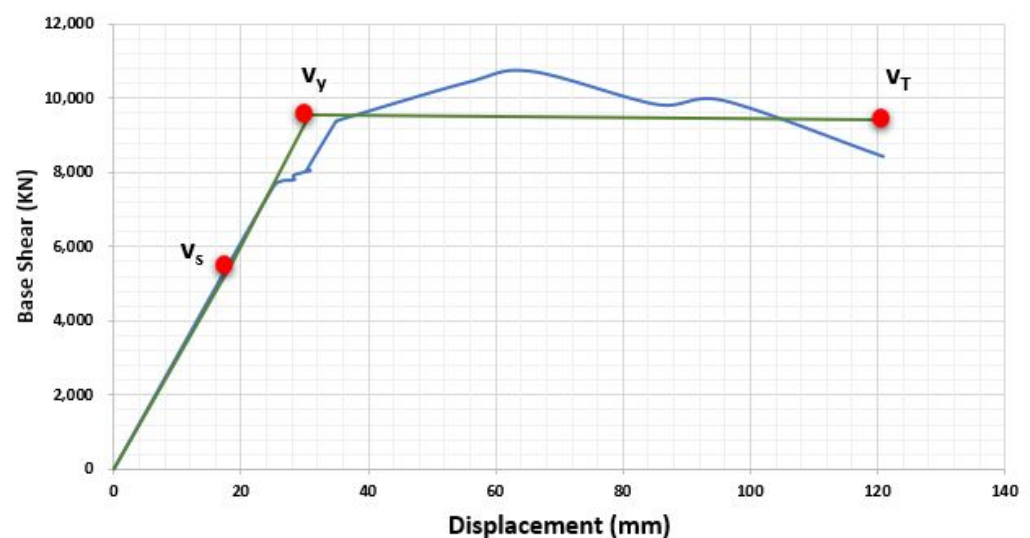


Figure 27. Mingora Bridge R-factor in longitudinal direction.

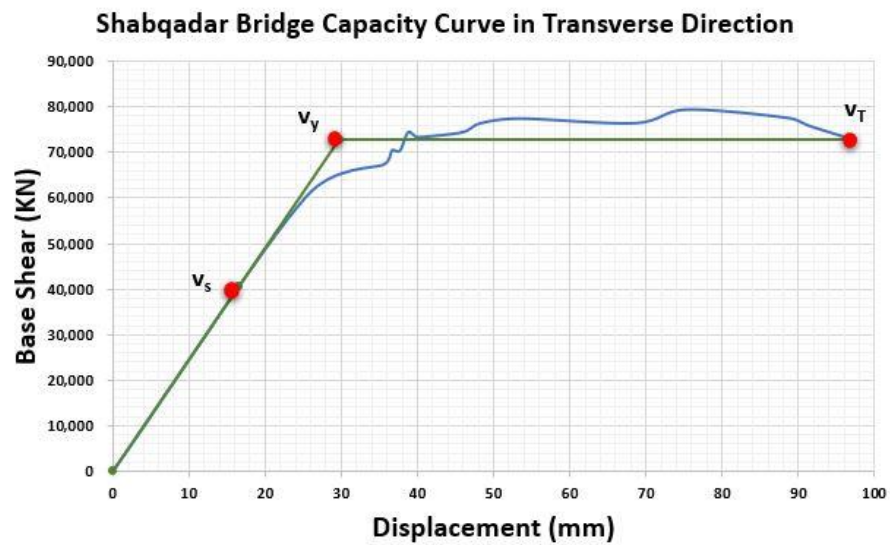


Figure 28. Shabqadar Bridge R-factor in transverse direction.

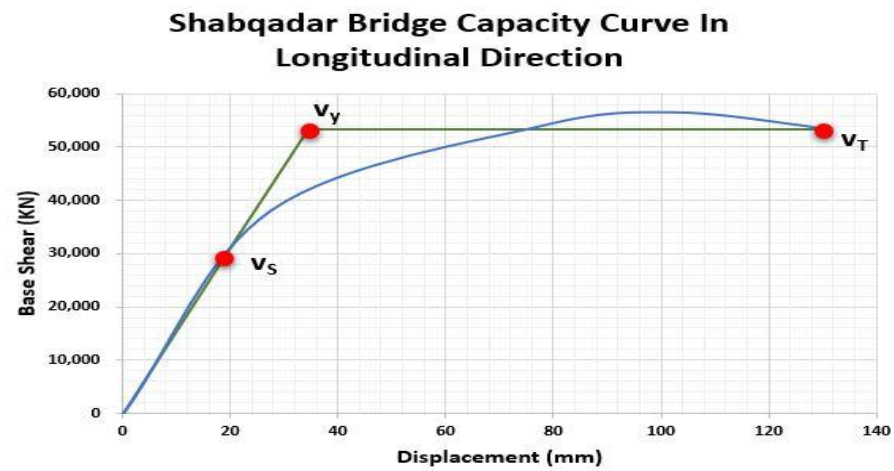


Figure 29. Shabqadar Bridge R-factor in longitudinal direction.

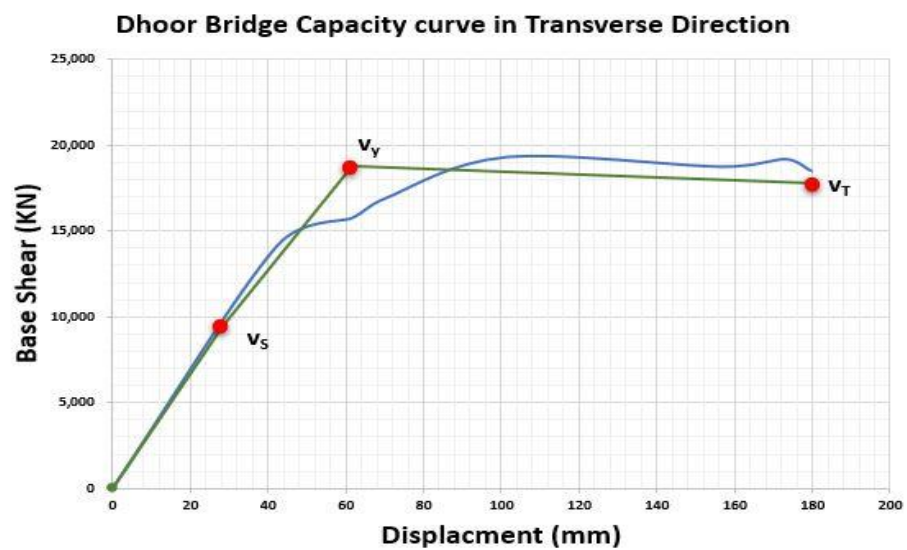


Figure 30. Dhoor Bridge R-factor in transverse direction.

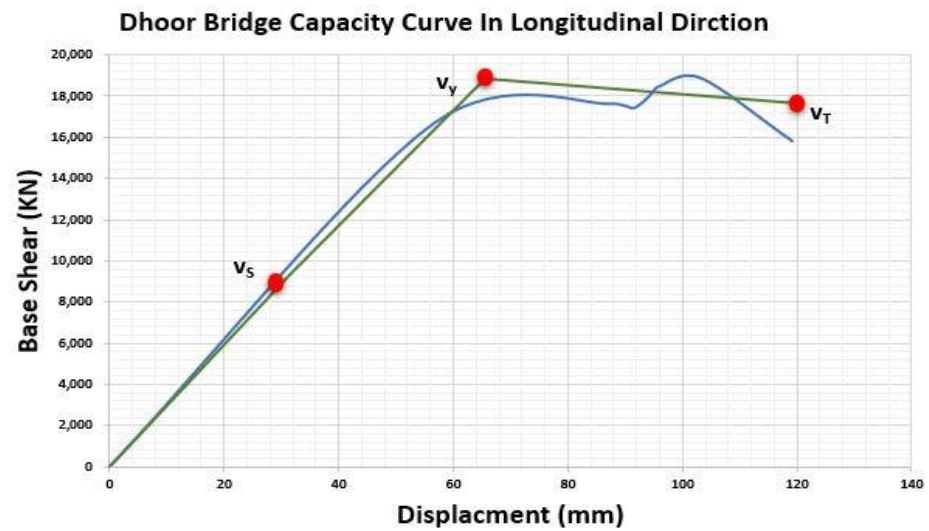


Figure 31. Dhoor Bridge R-factor in longitudinal direction.

Table 6. Mingora Bridge transverse direction co-efficient.

T	a	b	C (T, α)	μ	R_{μ}	Δ_m	Δ_y	Ω	R-Factor
0.47	1	0.42	1.20	3.52	3.18	120.56	34.59	1.71	5.41

Table 7. Mingora Bridge longitudinal direction co-efficient.

T	a	b	C (T, α)	μ	R_{μ}	Δ_m	Δ_y	Ω	R-Factor
0.47	1	0.42	1.20	3.39	3.08	118.65	34.501	1.45	4.48

Table 8. Shabqadar Bridge transverse direction co-efficient.

T	a	b	C (T, α)	μ	R_{μ}	Δ_m	Δ_y	Ω	R-Factor
1.44	1	0.42	0.88	2.97	3.14	97.14	32.68	1.74	5.47

Table 9. Shabqadar Bridge longitudinal direction co-efficient.

T	a	b	C (T, α)	μ	R_{μ}	Δ_m	Δ_y	Ω	R-Factor
0.677	1	0.42	1.02	3.79	3.74	130.58	34.43	1.46	5.48

Table 10. Dhoor Bridge transverse direction co-efficient.

T	a	b	C (T, α)	μ	R_{μ}	Δ_m	Δ_y	Ω	R-Factor
0.813	1	0.42	0.966	2.92	2.96	179.606	61.78	2.17	6.44

Table 11. Dhoor Bridge longitudinal direction co-efficient.

T	a	b	C (T, α)	μ	R_{μ}	Δ_m	Δ_y	Ω	R-Factor
0.808	1	0.42	0.966	1.83	1.84	120.18	65.50	3.06	5.64

It is well known that both Ω and R_{μ} range rather sketchily; taking the lowest among the values calculated for the longitudinal and the transverse directions in each bridge, Ω varies from 1.45 to 2.17, and R_{μ} from 2.96 to 3.74 as mentioned in Tables 12 and 13. It should also be noted that high R_{μ} values do not essentially agree with high Ω values.

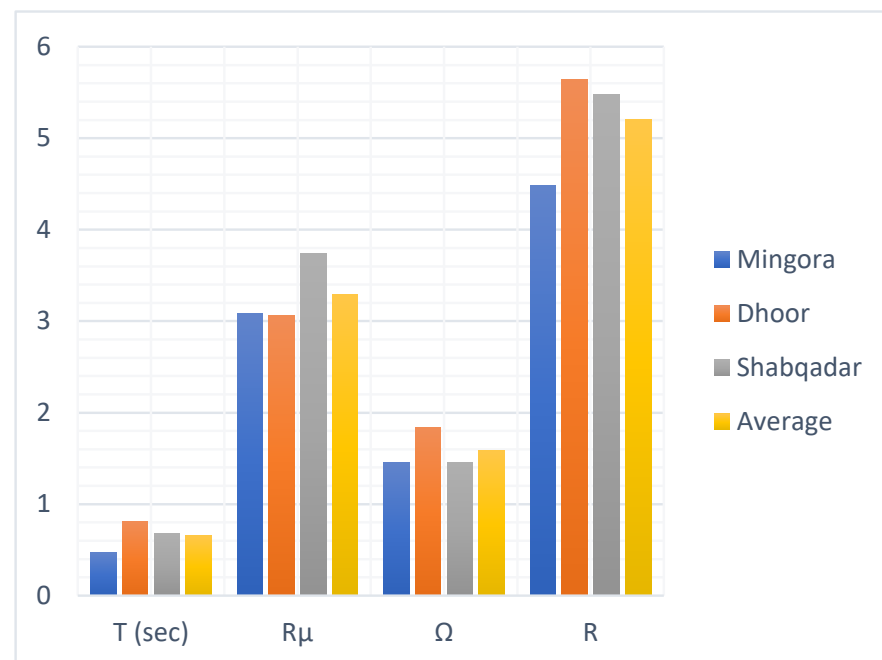
Table 12. Computed R-factor in longitudinal direction.

X-Dir	Bridge.1	Bridge.2	Bridge.3	Average
Name	Mingora	Dhoor	Shabqadar	
T (s)	0.472362	0.808817	0.67773	
R_{μ}	3.08	3.06	3.74	3.29
Ω	1.45	1.84	1.46	1.58
R	4.48	5.64	5.48	5.20

Table 13. Computed R-factor in transverse direction.

Y-Dir	Bridge.1	Bridge.2	Bridge.3	Average
Name	Mingora	Dhoor	Shabqadar	
T (s)	0.473977	0.81375	1.4434	
R_{μ}	3.18	2.96	3.14	3.09
Ω	1.71	2.17	1.74	1.87
R	5.41	6.44	5.47	5.77

The R-factor's calculated values, overstrength, and ductility factors in longitudinal and transverse directions are listed in Tables 4 and 5. R-factor in the longitudinal direction is 4.50, while in the transverse direction, it is 5.18. A comparison of R-factor in longitudinal and transverse directions is shown in Figures 32 and 33, respectively. These values are more than recommended as per AASTHO-LRFD, indicating the greater capacity of the bridges. The higher value of the R-factor in the transverse direction is as in AASTHO-LRFD. In the transverse direction, bridges are more resilient than in the longitudinal direction due to the presence of shear keys or the contribution of the substructure.

**Figure 32.** Comparison R-factor in longitudinal direction.

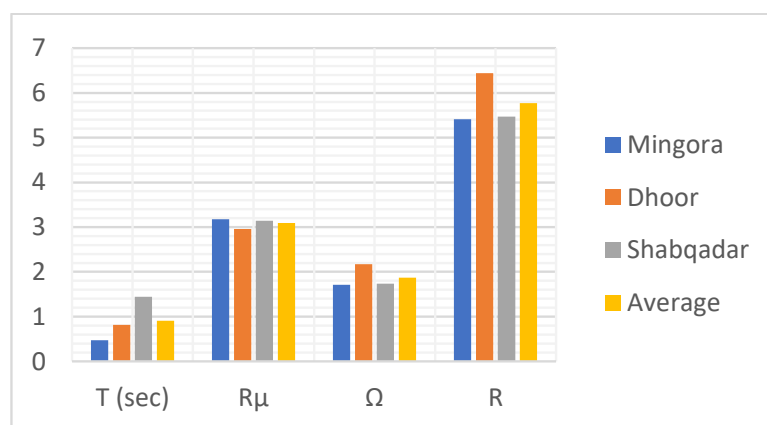


Figure 33. Comparison of R-factor in transverse direction.

5. Conclusions

This research article evaluated the R-factor for commonly found RC bridges in Pakistan. For this purpose, three existing RC simply supported bridges in Pakistan were modeled and analyzed using pushover analyses. The finite element model of these bridges was pushed both in a transverse and longitudinal direction. The prime goal of this paper was to determine the R-factor of bridges with elastomeric rubber bearing (ERB) pads. As a result, three prevailing bridges with ERB isolators were created between the superstructure and substructure. Because the superstructure of bridges has a high degree of rigidity, the substructure is responsible for ductility and energy dissipation. As a result, the type of substructure (single Piers, multiple Piers-bent, wall-type column, etc.), superstructure–substructure linking type (monolithic or isolated), and bearing behavior (linear and non-linear) play the most important roles in the energy dissipation mechanism and ductility of the entire bridge system. Because there is no energy dissipation at the bearing level in bridges with elastomeric rubber bearing (ERB) pads, seismic forces are carried to the substructure without reduction, and energy is dissipated through the production of plastic hinges in the column. As a result, the substructure of this type of bridge must have a more ductile behavior. The R-factor values improve as ductility improves. However, further research is needed to determine how the pier sections, the spacing between columns in the transverse direction, live load and traffic behavior, and the height of columns affect the R-factor values.

The average values of R-factors for the bridges with ERB are calculated as R-factor values varying between 4.56 and 5.89 in the longitudinal direction and have a mean value of 5.20. The R-factor for transverse direction ranges from 5.44 to 6.54, having a mean value of 5.77. R-factor in the longitudinal and the transverse direction is not similar. The R-factor obtained in this study is different from the AASTHO provisions (i.e., $R = 3/2 = 1.5$ in the longitudinal direction and $R = 5/2 = 2.5$ in the transverse direction). Therefore, the use of code-based R-factor values is conservative. Because of this, in the case of adopting ERB as the seismic isolation system, the non-linear behavior of the structure arises from the production of plastic hinges in the piers, and bridge design engineers tend to consider the non-linear behavior of the entire bridge structure in the seismic isolation system.

Author Contributions: Conceptualization M.J.B. and M.W.; data curation M.J.B., M.W. and M.A.S.; formal analysis M.W., M.A.S., M.M.S.S. and M.A.; funding acquisition M.M.S.S.; investigation M.J.B. and M.W.; methodology M.J.B., M.W., M.A.S. and M.A.; project administration M.A.S.; resources M.J.B., M.W., M.M.S.S. and M.A.; writing—original draft M.J.B., M.W. and M.A.S.; writing—review B.Z., M.M.S.S. and M.A. All authors have read and agreed to the published version of the manuscript.

Funding: The research is partially funded by the Ministry of Science and Higher Education of the Russian Federation as part of the World-class Research Center program: Advanced Digital Technologies (contract No. 075-15-2022-311 dated 20.04.2022).

Institutional Review Board Statement: Not Applicable.

Informed Consent Statement: Not Applicable.

Data Availability Statement: The authors declare that all data supporting the findings of this study are within the article.

Conflicts of Interest: All the authors have seen the final version of the paper and declared no conflict of interest.

References

1. Ali, S.M.; Khan, A.N.; Rahman, S.; Reinhorn, A.M. A survey of damages to bridges in Pakistan after the major earthquake of 8 October 2005. *Earthq. Spectra* **2011**, *27*, 947–970. [CrossRef]
2. Kawashima, K. Seismic Isolation of Highway Bridges. *J. JAEE* **2004**, *4*, 283–297. [CrossRef]
3. Sakellariadis, L.; Anastasopoulos, L.; Gazetas, G. Fukae bridge collapse (Kobe 1995) revisited: New insights. *Soils Found.* **2020**, *60*, 1450–1467. [CrossRef]
4. Putra, R.; Riyono, W.A. Risk analysis of seismic bridge damage: Case study after Lombok and Palu earthquake. In *E3S Web of Conferences 4th ICEEDM*; EDP Sciences: Les Ulis, France, 2020; Volume 156, p. 03008.
5. Memari, A.M.; Harris, H.G.; Hamid, A.A.; Scanlon, A. Ductility evaluation for typical existing R/C bridge columns in the eastern USA. *Eng. Struct.* **2005**, *27*, 203–212. [CrossRef]
6. Kanamori, H. The energy release in great earthquakes. *J. Geophys. Res.* **1977**, *82*, 2981–2987. [CrossRef]
7. Aye, M.N.; Kasai, A.; Shigeishi, M. An Investigation of Damage Mechanism Induced by Earthquake in a Plate Girder Bridge Based on Seismic Response Analysis: Case Study of Tawarayama Bridge under the 2016 Kumamoto Earthquake. *Adv. Civ. Eng.* **2018**, *2018*, 9293623. [CrossRef]
8. Government of Pakistan Ministry of Housing and Works. *Building Code of Pakistan*; Government of Pakistan Ministry of Housing and Works: Islamabad, Pakistan, 2007.
9. Ali, M. *BCP SP-2007 BCP SP-2007 Preface*; U.E.T Taxila: Rawalpindi, Pakistan, 2007.
10. Khan, S.; Waseem, M. Earthquake seismic site response analysis by comparison between equivalent linear and nonlinear methods, a case study at Kohat and Muzaffarabad. *J. Himal. Earth Sci.* **2019**, *52*, 46–63.
11. Khan, R.; Kumar, M.; Ahmed, M.; Rafi, M.; Lodi, S. Earthquake Damage Assessment of Bridges in Karachi. *NED Univ. J. Res.* **2015**, *12*, 45.
12. Constantinou, M.; Quarshie, J. *Response Modification Factors for Seismically Isolated Bridges*; PAHO: New York, NY, USA, 1998. Available online: <http://mceer.buffalo.edu/publications/catalog/reports/Response-Modification-Factors-for-Seismically-Isolated-Bridges-MCEER-98-0014.html> (accessed on 3 November 1998).
13. Federal Emergency Management Agency (FEMA). *NEHRP Guidelines for the Seismic Rehabilitation of Buildings and NEHRP Commentary on the Guidelines for the Seismic Rehabilitation of Buildings*; Federal Emergency Management Agency (FEMA): Washington, DC, USA, 1997.
14. International Conference of Building Officials. UBC-1997 Code. In *Uniform Building. 'Uniform Building Code'*; International Conference of Building Officials: Whittier, CA, USA, 1997; ISBN 1884590896.
15. Federal Emergency Management Agency (FEMA). *ATC-1978 Applied Technology Council. Tentative Provisions for the Development of Seismic Regulations for Buildings, National Science Foundation and National Bureau of Standards*; Federal Emergency Management Agency (FEMA): Washington, DC, USA, 1984.
16. Whittaker, A.; Hart, G.; Rojahn, C. Seismic response modification factors. *J. Struct. Eng.* **1999**, *125*, 438–444. [CrossRef]
17. Ran, N. ATC 19 Structural Response Modification Factors. 1995. Available online: <https://www.atccouncil.org/pdfs/atc19toc.pdf> (accessed on 24 May 1995).
18. Gastineau, A.J.; Wojtkiewicz, S.F.; Schultz, A.E. Response Modification Approach for Safe Extension of Bridge Life. *J. Bridg. Eng.* **2012**, *17*, 728–732. [CrossRef]
19. Gastineau, A.J.; Wojtkiewicz, S.F.; Schultz, A.E. Lifetime Extension of a Realistic Model of an In-Service Bridge through a Response Modification Approach. *J. Eng. Mech.* **2013**, *139*, 1681–1687. [CrossRef]
20. Routledge, P.J.; Cowan, M.J.; Palermo, A. Low-damage detailing for bridges—A case study of Wigram-Magdala Bridge. In *Proceedings of the 2016 NZSEE Conference, Christchurch, New Zealand, 14 November 2016*; pp. 1–8.
21. Warn, G.P.; Whittaker, A.S. Asce Property Modification Factors for Seismically Isolated Bridges. *J. Bridg. Eng.* **2006**, *11*, 371–377. [CrossRef]
22. Çavdar, E.; Özdemir, G.; Karuk, V. Modification in Response of a Bridge Seismically Isolated with Lead Rubber Bearings Exposed to Low Temperature. *Tek. Dergi* **2022**, *33*, 1–24. [CrossRef]
23. Zhang, F.; Li, S.; Wang, J.; Zhang, J. Effects of fault rupture on seismic responses of fault-crossing simply-supported highway bridges. *Eng. Struct.* **2020**, *206*, 110104. [CrossRef]
24. Bergami, A.V.; Lavorato, D.; Fiorentino, G.; Nuti, C. Incremental Modal Pushover Analysis (IMPA) for bridges. *Appl. Sci.* **2021**, *2911*–2919. [CrossRef]

25. Zhang, A.L.; Qiu, P.; Guo, K.; Jiang, Z.Q.; Wu, L.; Liu, S.C. Experimental study of earthquake-resilient end-plate type prefabricated steel frame beam-column joint. *J. Constr. Steel Res.* **2020**, *166*, 105927. [[CrossRef](#)]
26. Kappos, A.J.; Paraskeva, T.S.; Moschonas, I.F. Response Modification Factors for Concrete Bridges in Europe. *J. Bridg. Eng.* **2013**, *18*, 1328–1335. [[CrossRef](#)]
27. Zahrai, S.M.; Khorraminejad, A.; Sedaghati, P. Response modification factors of concrete bridges with different bearing conditions. *Earthq. Struct.* **2019**, *16*, 185–196. [[CrossRef](#)]
28. Waseem, M.; Spacone, E. Fragility curves for the typical multi-span simply supported bridges in northern Pakistan. *Struct. Eng. Mech.* **2017**, *64*, 213–223. [[CrossRef](#)]
29. Ali, S.M. Study of energy dissipation capacity of rc bridge columns under seismic demand. Ph.D. Thesis, University of Engineering and Technology, Peshawar, Pakistan, 2009.
30. Uang, C.-M. Establishing R (or R_w) and Cd factors for building seismic provisions. *J. Struct. Eng.* **1991**, *117*, 19–28. [[CrossRef](#)]
31. Aviram, A.; Mackie, K.; Stojadinovic, B. *Guidelines for Nonlinear Analysis of Bridge Structures in California*; Pacific Earthquake Engineering Research Center: Berkeley, CA, USA, 2008.
32. Akogul, C.; Celik, O. Effect of Elastomeric Bearing Modeling Parameters on the Seismic Design of RC Highway Bridges with Precast Concrete Girders. In Proceedings of the 14th World Conference on Earthquake Engineering, Beijing, China, 12–17 October 2008. Available online: https://www.researchgate.net/publication/265930567_Effect_of_elastomeric_bearing_modeling_parameters_on_the_Seismic_design_of_RC_highway_bridges_with_precast_concrete_girders (accessed on 17 October 2008).
33. *Caltrans Seismic Design Criteria, Version 1.3*; Caltrans: Sacramento, CA, USA, 2004.
34. Mander, J.B.; Priestley, M.J.N.; Park, R. Theoretical stress-strain model for confined concrete. *J. Struct. Eng.* **1989**, *114*, 1804–1826. [[CrossRef](#)]
35. Tortolini, P.; Petrangeli, M.; Lupoi, A. Criteri per la verifica e la sostituzione degli appoggi in neoprene di viadotti esistenti in zona sismica. In Proceedings of the 14th Italian Conference on Earthquake Engineering, Bari, Italy, 30 August–3 September 2011. Available online: <https://www.researchgate.net/publication/266941512> (accessed on 17 October 2008).
36. Malhotra, V.M.; Mehta, P.K. Standard specifications. In *Pozzolanic and Cementitious Materials*; CRC Press: Boca Raton, FL, USA, 2006; p. 871. [[CrossRef](#)]
37. Yazdani, N.; Eddy, S.; Cai, C.S. Effect of bearing pads on precast prestressed concrete bridges. *J. Bridg. Eng.* **1999**, *5*, 224–232. [[CrossRef](#)]
38. Shafiei-tehrany, R. Nonlinear Dynamic and Static Analysis of I-5 Ravenna Bridge. Ph.D. Thesis, Washington State University, Washington, WA, USA, 2008.
39. Muthukumar, S. *A Contact Element Approach with Hysteresis Damping for the Analysis and Design of Pounding in Bridges*; Georgia Institute of Technology: Atlanta, GA, USA, 2003.
40. *Caltrans Seismic Design Criteria, Version 1.7*; Caltrans: Sacramento, CA, USA, 2013.
41. Hakim, R.A.; Alama, M.S.; Ashour, S.A. Seismic Assessment of RC Building According to ATC 40, FEMA 356 and FEMA 440. *Arab. J. Sci. Eng.* **2014**, *39*, 7691–7699. [[CrossRef](#)]
42. Favvata, M.J.; Naoum, M.C.; Karayannis, C.G. Seismic Evaluation of Infilled RC Structures with Nonlinear Static Analysis Procedures. In Proceedings of the 15th World Conference on Earthquake Engineering, Lisbon, Portugal, 24–28 September 2012.
43. Abdi, H.; Hejazi, F.; Jaafar, M.S. Response modification factor—Review paper. *IOP Conf. Ser. Earth Environ. Sci.* **2019**, *357*, 1–16. [[CrossRef](#)]
44. Building Seismic Safety Council; Washington, D. *NEHRP Recommended Provisions for Seismic Regulations for New Buildings*; U.S. Department of Homeland Security: Washington, CA, USA, 1988.
45. Zafar, A. Response Modification Factor of Reinforced Concrete Moment Resisting Frames in Developing Countries. Master’s Thesis, University of Illinois at Urbana-Champaign, Champaign, IL, USA, 2009.
46. Nassar, A.A.; Krawinkler, H. Seismic demands for SDOF and MDOF systems, Report No. 95. *Stanford Univ.* **1991**, *204*, 12–45.
47. Krawinkler, H.; Seneviratna, G.D.P.K. Pros and cons of a pushover analysis of seismic performance evaluation. *Eng. Struct.* **1998**, *20*, 452–464. [[CrossRef](#)]
48. Fajardo, K.N.; Blázquez, A. *FEMA 356 Preestándar y Comentario Para la Rehabilitación Sísmica de Edificios*; Interreg Poctefa: Spain, France, 2000; p. 519.
49. Najam, F.A. Nonlinear Static Analysis Procedures for Seismic Performance Evaluation of Existing Buildings—Evolution and Issues. In *International Congress and Exhibition Sustainable Civil Infrastructures: Innovative Infrastructure Geotechnology*; Springer: Cham, Switzerland, 2018. [[CrossRef](#)]
50. ATC 40—Seismic evaluation and retrofit of concrete buildings. Available online: <https://www.atcouncil.org/pdfs/atc40toc.pdf> (accessed on 30 November 1996).
51. FEMA-440, Improvement of Nonlinear Static Seismic Analysis Procedures. Available online: https://store.atcouncil.org/index.php?dispatch=attachments.getfile&attachment_id=123 (accessed on 29 June 2005).